P. Schattenberg

Improving Satellite Positioning By Measuring Eclipse Times

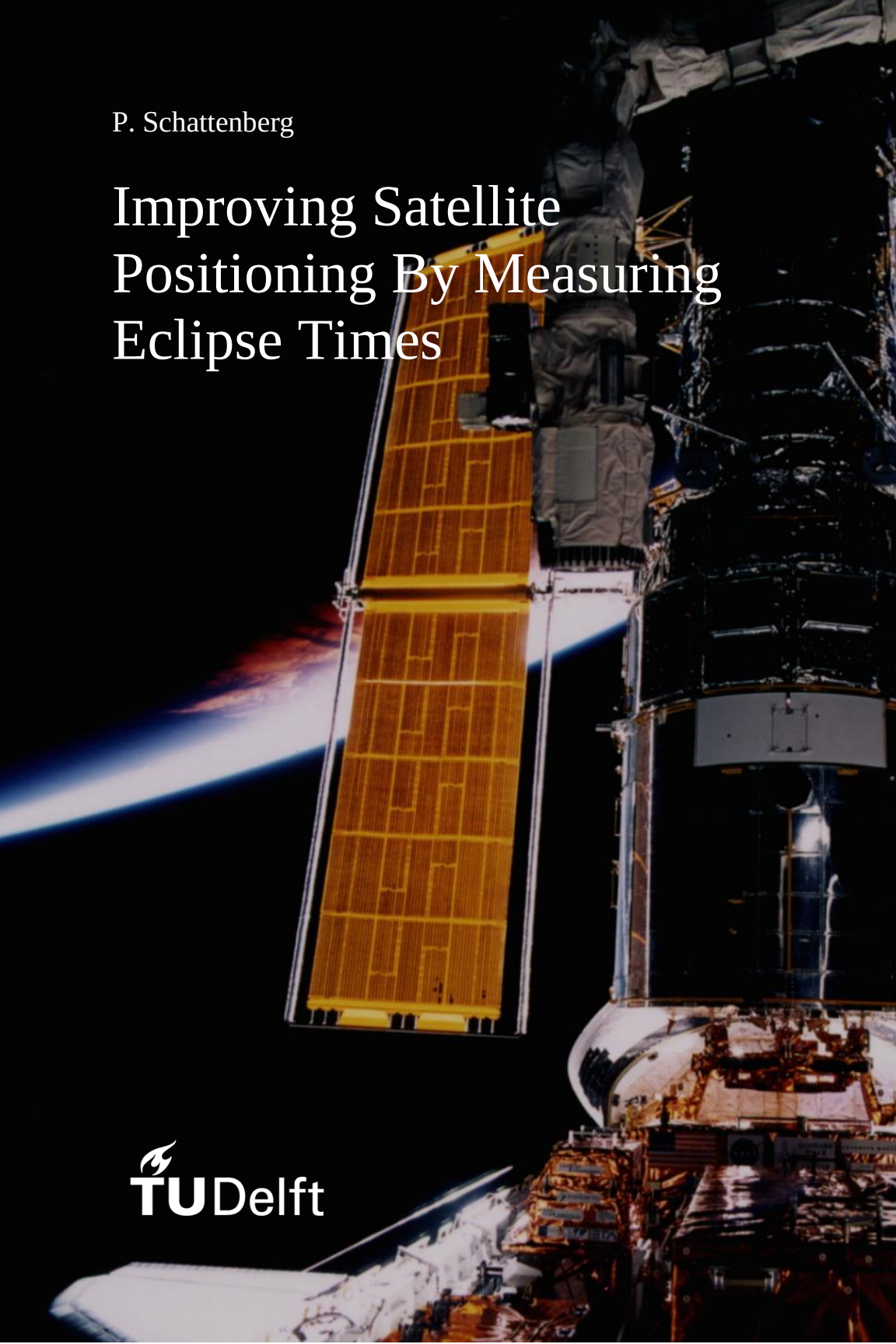

TU Delft

Improving Satellite Positioning By Measuring Eclipse Times

By:

P. Schattenberg

in partial fulfilment of the requirements for the degree of

Masters of Science
in Aerospace Engineering

at the Delft University of Technology,
to be defended on Tuesday, October 31, 2017 at 10:00 AM.

Supervisor	ir. P. Sundaramoorthy
Thesis Committee	Dr. ir. B. Root, TU Delft
	ir. B. Zandbergen, TU Delft

Typeset in Garamond and Arial
Microsoft Visio graphics support by A.I. van Hengel
Printed and bound by Lulu Press, Inc., Raleigh, USA

First Printing: 2017

1 2 3 4 5 6 7 8 9 10

"To infinity and beyond."
Buzz Lightyear

Table of Contents

List of Figures

List of Tables

Preface

Ever since I can remember, I have always been interested in flying and spaceflight. When I was three, I was asked what I wanted to be when I grew up. My answer was first to "be like my dad and fix electricity" and then be an astronaut.

There are two vivid memories that played a major role in getting me to where I am today. One teacher particularly stands out, Mrs. Susan Cutler. Derek Muller summarized what I believe the fundamental role of a teacher is quite well when he said that "the job of a teacher is to inspire, to challenge, [and] to excite their students to want to learn." When Mrs. Cutler brought our 3rd grade class in from recess to watch a space shuttle launch on television, she did just that. This was a first for us all and really got me excited about spaceflight. My father also played a major role in this as well by us spending our father-son time building and launching model rockets on the weekends. These two events, as well as the culmination of many other events, really got me looking up and set my sights towards the stars.

Reflecting on one's life, it is easy to see how certain events really shape one as a person and how one event leads to another to get them to where they are today. As I have come to learn: hindsight is always twenty-twenty. I would not be the person I have become without the help, support, and guidance of my family, friends, teachers, and mentors. And for this, I owe them a lot of thanks and gratitude. I especially thank my father and mother, Carl and Lauri Schattenberg, for their never-ending encouragement and support in helping me realize my dreams, challenging me to succeed, and for countless proofreading sessions throughout the years. Thank you!

To me, this thesis marks a milestone in being one step closer to the stars and the beginning of a new chapter in my life. I do not know what that new chapter might entail, but no matter what it is, I have a good feeling about it.

P. Schattenberg
Delft, October 2017

Abstract

More than forty years after its introduction, Simplified General Perturbation Theory No. 4 (SGP-4) is still currently in use as the de facto standard in orbit propagation and in generating Two-Line Elements (TLEs). Unfortunately, the positioning error that results from the generated TLEs have remained relatively unchanged and continue to increase with larger TLE update intervals. This paper investigates an approach in analyzing truth data to help in possibly minimizing the errors associated with generated TLEs. The current resulting positioning errors are permissible for general tracking of satellites and pass scheduling; however, the errors that result from SGP-4 alone can cause some limitations if used in other applications. This is not necessarily a challenge for large satellites that can afford to include certain instruments to help keep positioning errors low, but due to the power, volume, and cost limitations of small satellites, this can become problematic as there are not as many sensors that can fit within the small form factor. Therefore, shadow time characteristics for Low-Earth Orbit (LEO) satellites will be examined to hopefully improve TLE accuracies by incorporating measured shadow time.

1 Introduction

"Imagination will often carry us to worlds that never were. But without it we go nowhere."

Carl Sagan

The space industry is a very conservative field with analytical orbital propagators that date back to at least three decades. These orbit propagators are still widely used today for not only tracking satellites, but also in generating *Two-Line Elements* (TLEs) for dissemination to the general public. When using TLEs in conjunction with these orbit propagators, as long as the time interval remains relatively small, the propagated position estimate errors remain small as well; however, as this time interval increases, so do positioning estimate errors of satellites.

Currently, in order to keep these errors low, tracking stations that generate TLEs need to maintain a regularly-spaced schedule in tracking satellites to regenerate their TLEs. This needs to be done not just for one satellite, but for all functional satellites as well as any man-made object orbiting Earth that no longer serves a useful purpose. This ultimately results in thousands of cataloged space objects that need to be tracked on a daily basis.

As satellites become smaller, their ability to be tracked to the same level of precision as larger satellites decreases. This makes it difficult to maintain an accurate position estimate on smaller satellites and greatly increases the probability and risk of a possible collision. This is not only a problem for small satellites, but larger satellites as well. For example, on February 11, 2009, an Iridium communication satellite collided with a non-functioning Russian satellite, which resulted in both satellites being destroyed. This created a large field of debris that further endangered other orbiting satellites, including the International Space Station (ISS). As a result, the U.S. Space Surveillance Network now tracks all satellites and debris objects larger than 10 centimeters (NASA Orbital Debris Program Office 2009). Occurrences like this could have been known ahead of time or avoided. If positioning estimate errors are kept as small as possible, the location of a satellite can be predicted into the future with a higher certainty, result in better measurement data, and allow for the ability to react upon an impending collision.

For small satellites, this is also the case; however, small satellites are difficult to track. Not only that, but they seem to have a larger covariance in positioning estimates (Figure 3-2). Couple this with the constraint of a small power, mass, volume and cost budget, positioning estimates of small satellites definitely leaves a door open for possible improvements. Therefore, a desirable solution should be sought after that stays within these constraints.

1.1 GENERAL INTRODUCTION

Even today, the smallest obtainable positioning errors by use of RADAR or optical measurements for Low-Earth Orbit (LEO) satellites are still relatively high (Table 1-1) and is still in the order of a couple hundred meters (Figure 1-1). Unfortunately, this error is only for the initial refined Two-Line Element set. If the TLE is not regularly updated, the effects of the simplified dynamics in the Simplified General Perturbation series propagators, as defined in *General Perturbations Theories Derived from the 1965 Lane Drag Theory* (Lane and Hoots 1979) and *Spacetrack Report No. 3* (Hoots and Roehrich 1980), start to dominate, and over the course of a

day, positioning uncertainties can grow at a rate of one to three kilometers a day (Vallado, et al. 2006) (Vallado and Agapov 2010).

Furthermore, with over a thousand active satellites and over half-a-million cataloged space debris objects, spaceflight is a very risky environment. Therefore, with large positioning estimate errors, Earth-orbiting satellites have to either execute debris avoidance maneuvers, if capable, or risk collision. For this reason, it is imperative to have systems in place for 1) generating TLEs with the smallest errors possible and a system where 2) the two-line elements are updated on a frequent basis. These two systems help to provide the best possible positioning estimates of satellites while keeping positioning errors low. This thesis explores an alternative option that uses onboard measurements to supplement the TLE data to improve upon positioning accuracy.

Table 1-1. Common Errors Associated with Orbit Determination. Note: RADAR errors were determined by using equation 8.8 in Curry's publication for a 1-degree beamwidth, S/R of 12, and km value of 1.6. C is the Speed of Light and B is defined as the signal bandwidth. (Curry 2004, 166-170) Typical values for RADAR Altitude measurements are about 10 meters (Vetter 2007, 141). Optical Source: Orbit Determination Results from Optical Measurements (Vallado and Agapov 2010).

ERROR SORUCES	ERROR (RMS)		
	RADAR	**Optical**	**Laser**
Cross-Track	~400 meters	250 – 500 meters	N/A
Along-Track	~400 meters	500 – 700 meters	N/A
Altitude	$\frac{c}{2B}$ ~ 10 meters	400 – 1000 meters	5 centimeters
TLE (After the Differential Correction Process)	± 200 to 500 meters		
Each Additional Day without updating a TLE	An absolute error of an additional 1 to 3 kilometers		

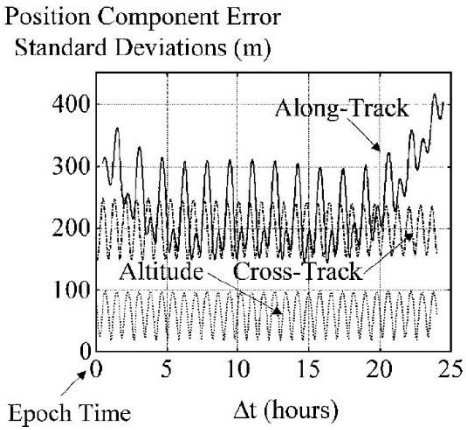

Figure 1-1. Positioning Estimation-Error Resulting from Magnetometers and Sun Sensor Data. Adapted from "Autonomous Low-Earth-Orbit Determination from Magnetometer and Sun Sensor Data" by M. Psiaki, 1999, *Journal of Guidance, Control, and Dynamics*, *27, 2*, p. 302. Copyright 1999 by M. Psiaki.

1.2 RESEARCH OBJECTIVE

The objective of this thesis project is to:

Improve upon the position estimate of satellites by supplementing Two-Line Elements with eclipse time data.

In other words, the purpose of this thesis is to determine if eclipse time data from a satellite's orbit can be used to decrease the positioning estimate error for that particular satellite. As previously stated, this will help in determining the location of a satellite with a higher certainty and hopefully result in higher-resolution data with location-dependent measurements. Therefore, the following two characteristics should be met:

- If a sensor does not exist, the **requirements** for such a sensor **will be developed**.
- The algorithm should be developed in a manner that is **simple** and **easy** to implement.

1.3 RESEARCH QUESTIONS

The research objective is realized by answering the questions presented below:

1. How can the positioning estimates for small satellites, and inherently low-cost satellites, be improved?
    a. Is there some piece of orbital information that can be used to improve upon positioning estimates?
    b. What parameters are influenced by this information?
    c. What are the requirements of such an instrument?
    d. Can the positioning error of the satellite be improved with this additional information?

These questions are used to establish a theoretical approach and serve as a basis in developing a solution to the research objective presented in Section 1.2.

1.4 RESEARCH METHODOLOGY & THESIS OUTLINE

This thesis is broken up into several parts: In Chapter 2, some background information is presented on cross-track, along-track, and radial errors. Also, Chapter 2 explores some of the current on-board systems used to derive orbital elements in small satellites. In Chapter 3, the tools that are used for analysis are explained individually. Together, these tools make up the toolkit used in analysis and are presented as close as possible in the order they were used. Chapter 4 describes how NASA's General Mission Analysis Tool (GMAT) was configured for analysis of shadow times and how it compares to the SGP-4/SDP-4 propagator. Furthermore, this chapter covers how analysis was carried out on MATLAB. Finally, the results of all this analysis are summarized and explained in Chapter 5 as well as recommendations for future follow-up work.

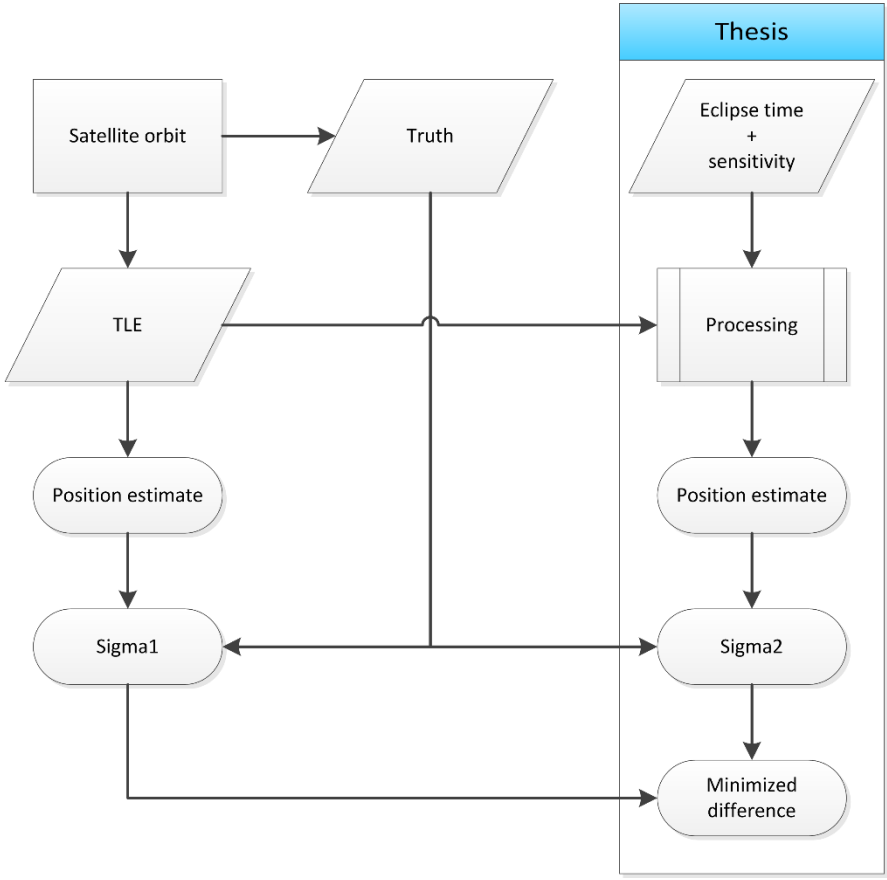

Figure 1-2. Thesis Process Structure.

Figure 1-2 shows the process used for analyzing Two-Line Elements. This zoomed-out graphic is presented in more detail in Section 4.2 and represents the methodology used in processing data and coming to the results presented in Chapter 5. In short, Precise Orbit Determination datasets obtained from the Technical University of Delft for Low-Earth Orbit satellites (namely, GOCE, CHAMP, and GRACE-A) was used in conjunction with publicly-available Two-Line Elements. Having this true positioning data is valuable as not all satellites have it generated for them. GOCE, CHAMP, and GRACE-A satellites are all relatively large satellites and can easily accommodate for measurement systems that would be difficult, if not impossible, to fit inside a small satellite.

Anyways, with this precise orbit determination data, the theoretical eclipse times can be calculated from TLEs and compared with the true eclipse times. With this information, errors can be formed between the data generated from the theoretical flight-path (from TLEs) and the actual flown path (from truth data). These errors are referred to in Figure 1-2 as *Sigma1* and *Sigma2*.

No matter what, the satellite will fly their real flightpath and not that of the TLEs. This is important in turning the problem around and simulating measured data by using data derived from true data and applying offsets to this derived data (*eclipse time* + *sensitivity* in Figure 1-2) to determine if a minimized difference in one of the edited orbit parameters can be achieved with respect to one of the Keplerian orbit parameters. Can an orbital parameter that is more closely related to the true Keplerian orbit be realized? The answer to this question is explored within this thesis.

2 Background Information

"Space is only 80 miles from every person on earth – far closer than most people are to their own national capitals."

Daniel Deudney

Before exploring the research objective and research questions as presented in Section 1.2 and 1.3, respectively, it is imperative to introduce some of the current ways on how Two-Line Elements are formed. An overview of various methodologies for ground-based observations to generate TLEs is covered in *An Overview on Orbit Determination Techniques for TLE Generation* (Schattenberg 2017) and in the sources contained within this publication. Therefore, this information will not be presented here. Instead, a very brief summary of techniques used on-board satellites will be presented as well where some of the sources of errors associated with along-track, cross-track, and radial positions and velocities stem from.

2.1 SOME SOURCES OF ERROR

Positioning errors from TLEs are still relatively large (Park, et al. 2010) (Vallado and Agapov 2010) (Vetter 2007) and if not continually updated, increase every day. Thus, accurately knowing the position of the satellite is key in generating an accurate TLE. However, some things need to be considered in TLE generation to keep errors low.

As most satellites do not have a cross-track velocity component, the cross-track errors are usually the smallest and remain the most stable (Vallado and Agapov 2010, 7). However, as a satellite is propagated forward in time, cross-track positioning uncertainties stem from two main sources: the inclination and right ascension of the ascending node of the satellite. Luckily, the inclination of the satellite remains relatively stable, but due to small fluctuations in the oblateness of Earth and third-body perturbations, the right ascension of the ascending node drifts with J2 perturbations having the largest effect for LEO Satellites (Wertz, et al. 1997, 270) (Larson and Wertz 1998, 140-142). This, in turn, causes a constant change and oscillation in positioning uncertainty in the cross-track position component.

When it comes to along-track errors, there are two main sources: drag and time synchronization. Drag forces primarily dominate orbits below 800 kilometers (Wertz, et al. 1997, 270). Thus, satellites constantly have to fight against this force. This makes time synchronization just as important for ground-based orbit determination systems as well as satellite-based orbit determination systems, due to the along-track direction experiencing very high velocities. Thus, any offset in clock times has the potential to cause large positioning errors in this direction.

The altitude and semi-major axis of the satellite can be determined by either using RADAR measurements or laser ranging. Using a laser, a satellite's altitude can be determined to about five centimeters (Vallado and Agapov 2010), and with RADAR, for altitude measurements, to about 10 meters (Curry 2004, 170). Using laser measurements requires a retro-reflector measuring at least 10 by 10 by 4.8 centimeters (Neubert, Grunwaldt and Neubert n.d.) and is thus unfit for small satellites that are, for example, 10 by 10 by 30 centimeters or smaller. As for RADAR measurements, it depends on the size of the satellite. Small satellites usu-

ally rely on low-gain omnidirectional antennas and make the satellite appear larger than it actually is. This interaction of the antenna as well as the shape and size of the satellite, and material used can lead to the uncertainty in RADAR measurements. (Speretta, Sundaramoorthy and Gill 2017)

Other sources of errors, along with their explanation concerning Orbit Determination systems, are found in *Mission Geometry; Orbit and Constellation Design and Management* (Wertz, et al. 2001, 270). An explanation of these, individually, is beyond the scope of this report, as most of them are already accounted for in the algorithms described in the aforementioned source and in *An Overview on Orbit Determination Techniques for TLE Generation* (Schattenberg 2017).

2.2 CURRENT SYSTEMS USED IN ON-BOARD ORBIT DETERMINATION

Orbit determination of a satellite allows for the calculation of six independent orbital parameters. Simply put, observations need to be made so that these six parameters can be derived. These observations can be done from ground-based measurements or by measurements taken onboard a satellite. For ground-based measurements, these methods include optical observations and radio-based measurements. These are explained further in detail in *Single-Station Tracking for Orbit Determination of Small Satellites* (Hart n.d.). As for satellite-based measurements, the selection seems to be rather limited to two choices: GPS (Jäggi n.d.) and from using a magnetometer in conjunction with sun sensor data. An explanation on using a magnetometer with sun senor data is beyond the scope of this report and can be found in detail in Psiaki's paper titled *Autonomous Low-Earth-Orbit Determination from Magnetometer and Sun Sensor Data* (Psiaki 1999).

As for the use of GPS, two important pieces of information for orbit determination are required: onboard time-synchronization and the latitude, longitude, and altitude of the satellite. By having this timestamped geocoded information, these latitude, longitude, and altitude measurements can be converted into other reference frames that are useful in

deriving orbital elements (i.e. Equation 4-14 in *Department of Defense World Geodetic System 1984* (National Imagery and Mapping Agency 2000)).

Algorithms exist for dynamic orbit determination and prediction for GPS and can produce position estimates with an accuracy ranging from 15 to 100 meters. However, these numbers are for a GPS receiver specifically developed by the *Deutsches Zentrum für Luft- und Raumfahrt* (DLR) for a particular satellite presented in a report titled *High-Precision Onboard Orbit Determination for Small Satellites* (Gill, et al. 2004).

When wanting to use a commercial-off-the-shelf GPS receiver instead, more problems arise due to export regulations across international borders posing operational limitations on operational altitudes and speeds. These regulations, commonly referred to as ITAR (The International Traffic in Arms Regulations) can be found in 22 CFR 120-130.

Therefore, due to this limited choice of satellite-based measurements for orbit determination and ITAR restrictions, a solution is sought after that is capable of deriving at least one of these six independent orbital parameters that does not rely on GPS positioning information.

3 Theoretical Approach

"Don't dilly-dally, Paul!"

Susan Cutler

This chapter is broken up into two separate parts. In Section 3.2, algorithms that have already been develop are presented as well as any reasoning behind why certain choices were made. This includes orbit propagators, date representation, conversion of coordinates, and extracting information from timestamped data. In Section 3.3, two analytical solutions are examined in calculating the theoretical eclipse time – that is, the theoretical time a satellite will spend in the shadow of Earth. Unfortunately, there seems to be an apparent lack in literature for a non-numerical-integration-based solution for an *Conical Shadow Model.* Therefore, an analytical-based solution was developed as a first-order approximation in calculating umbral eclipse times and is presented in Section 3.3.2. The errors associated with these two analytical solutions are then compared and the results are presented in the section that follows.

The tools used for analysis are explained individually within their respective subsection. When combining Section 3.2 and 3.3 together, they make up the toolkit used in analysis as setup in Chapter 4 and in present-

ing the results in Chapter 5. In the following subsections, the tools are presented as close as possible to the order in which they were used.

3.1 BACKGROUND INFORMATION

Two-line elements have historical roots dating back to the 1960s with the *Transmission Format* still serving as the *de facto* standard format for distributing and updating information concerning orbits of satellites. This format, as defined in *Spacetrack Report No. 3* (Hoots and Roehrich 1980), distributes the bare minimum information needed to calculate the location of a satellite and accurately propagate its orbit. Six elements are needed to define an orbit. Five of them are given directly on the two-line elements, and one of them, the semi-major axis, a, is directly calculated from the mean motion – see equations for a_1 in *Spacetrack Report No. 3* (Hoots and Roehrich 1980) – in order to recover all six Keplerian orbital elements. These six Keplerian elements are sufficient to calculate the position and velocity of the spacecraft at the time specified in the element set; however, they alone are not sufficient if the location of the satellite is to be calculated at another instant in time. In the remainder of this chapter, the tools used in examining the theoretical eclipse time of satellites are outlined.

3.2 TOOLS FOR ANALYSIS

Here within, algorithms that have already been developed and standard formats for positioning data are presented.

In Section 3.2.1, the precise orbit determination format for data generated by personnel at the Technical University of Delft are briefly explained.

Section 3.2.2 explores the reasoning behind why the SGP-4/SDP-4 propagator was selected as the propagator of choice, and in the following section (Section 3.2.3), the errors associated between propagating one TLE to the timestamp of the TLE that follows are studied. Doing so allows for a table of errors to be constructed to determine if any of the orbital element could be improved upon.

Lastly, Sections 3.2.4 to 3.2.7 explain a date representation, coordinate system transformations, and how to take three position vectors at three

different timestamps to estimate the velocity of the spacecraft at the second observed position.

The tools are explained in more detail below and are presented as close as possible to the order in which they were used.

3.2.1 Truth Data

In analysis of shadow times, truth data was used for determining the orbital elements of a satellite at a specified time that was supplied by personnel in the Space Exploration Department at the Technical University of Delft. This data consists of the x-, y-, and z-component in position and velocity in the International Terrestrial Reference Frame as defined on the ITRF Website (Institut National de L'information Geographique et Forestiére 2016).

The satellites GOCE, GRACE-A, and CHAMP were used in this analysis. These satellites, though large, have their orbits well-defined and are flying at similar altitudes to that of smaller satellites, and therefore still provide valuable data in determining the maximum uncertainty in eclipse times for small satellites. The precise orbit determination positioning data provided by the Technical University of Delft was supplied on a per-satellite basis at an "orbit precision at the level of a few centimeters" (Doornbos 2017).

What this orbit-precision-level means is that if any improvements in the positioning of a satellite by measuring shadow times can be made, they can be improved up to an uncertainty of about a few centimeters in the respective reference frame; however, the astronomical constants presented in the orbit propagator mentioned in Section 3.2.2 are expressed in the WGS84 reference frame (Hoots and Roehrich 1980). Luckily, this reference frame is "coincident with ITRF at about [the] 10-centimeter level…This means that one can consider that ITRF coordinates are also expressed in WGS84 at 10 cm level" (Quality Positioning Services 2016). Therefore, ultimately if no conversion is made between the two reference frames and if improvements are done in the meter-resolution, the smallest uncertainty that results in converting reference frames can be considered negligible.

3.2.2 Orbit Propagator Selection

Originally, two propagators were implemented for analysis of TLEs: SGP and SGP-4. The latter of the two propagators became the choice for TLE propagation and analysis within this report. The other propagators, AFGP-4, IGP-4, SDP-4 and SGP-8/SDP-8, were not implemented. Before beginning, it is worth noting that the *4* or *8* does not necessarily mean that this type of propagator is better than the other lower-numbered or non-existent-numbered propagators. Simply put, it means that it is either the 4^{th} or 8^{th} theory in the Simplified General Perturbation (SGP) theory set. With that said, the reasoning behind why the SGP-4 algorithm was chosen for this thesis is presented below.

The decision to use the Brouwer-based model, Simplified General Perturbation Theory #4 (SGP-4), mainly stems from two sources:

1. a report to U.S. Congress on *NORAD's Information Processing Improvement Program* (Staats 1978), and
2. a report where *Spacetrack Report No. 3* (Vallado, et al. 2006) is re-examined.

The NORAD report examined the performance of five different orbit propagation algorithms (DP-4, SGP-4, IGP-4, AFGP-4, and Special Perturbations) based on two criteria: *accuracy* and *speed* (Figure 3-1). Staats states "that it was planned that all space objects would be tracked with AFGP-4 accuracy; however, due to the limited capacity" of the Space Computation Center's (SCC) two Honeywell 6080 mainframe computers, DP-4 and SGP-4 would be used to "keep the SCC orbital catalog for most of the [tracked satellites]." (Staats 1978, 17-18). For this reason, the Space Computation Center settled upon using the *DP-4* and *SGP-4* algorithms as their standard even though higher-accuracy models existed. These models, DP-4 and SGP-4, are in fact *simplifications* of the AFGP-4 model (Lane and Hoots 1979). To date, there seems to be a lack of literature on the higher-accuracy algorithms without any source code on these algorithms, and thus assessing the performance of IGP-4 and AFGP-4 cannot be performed and is beyond the scope of this report. Thus, SGP, SGP-4/SDP-4, and SGP-8/SDP-8 still remain as possible candidates for this thesis. However, this will be narrowed down even further.

Program symbol	Accuracy	Speed
DP-4	Low	High
SGP-4	Low	High
IGP-4	Medium	Medium
AFGP-4	High	Low
Special Perturbations	Very high	Very low

Figure 3-1. Speed and Accuracy Comparison between Different Orbit Propagators. Adapted from NORAD's Information Processing Improvement Program, 1978, Copyright 1978 by Elmer B. Staats.

At the time Spacetrack Report No. 3 was written, Vallado, et al. state that SGP was replaced by the SGP-4/SDP-4 algorithms without any reason given. Nevertheless, the release of this report officially introduced five orbital propagation models, SGP, SGP-4/SDP-4, and SGP-8/SDP-8, and resulted from a "user compatibility survey of space surveillance operational sites and official users" (Vallado, et al. 2006, 1). Furthermore, Vallado, et al. goes on to state that time and consideration was indeed given to replace SGP-4/SDP-4 by SGP-8/SDP-8 as the standard satellite model in order to alleviate deficiencies concerning special cases of orbital decay and reentry (Vallado, et al. 2006, 2). However, they noted that "there is [still] no evidence to suggest that SGP-8/SDP-8 was implemented for operational TLE formation" even though the element sets that would be generated by SGP-8 would still be compatible with the previously mentioned propagators (Hoots and Roehrich 1980, 2).

For these reasons, the initial list of orbit propagators – AFGP-4, IGP-4, SGP, SGP-4/SDP-4, SGP-8/SDP-8, and Special Perturbations – have now been narrowed down to the propagator of choice: SGP-4/SDP-4. This selection also keeps with a *common practice* of using SGP-4 for tracking satellites. Furthermore, the NORAD element set is generated using the SGP-4/SDP-4 orbital model and by using any other model, different positioning estimates would result (Kelso 2014). Also, and there is no evidence to suggest otherwise that another propagator is used as the *de facto* standard for TLE formation (Vallado, et al. 2006) (D. A. Vallado 2007, 692).

More information on the differences between all of these propagators can be found in *An Overview on Orbit Determination Techniques for TLE Generation* (Schattenberg 2017). More information on the derivation and development of these algorithms can be found in (Kozai 1959), (Brouwer 1964), (M. H. Lane 1965), (Lane and Crawford 1969), (Lane and Hoots 1979), (Hoots and Roehrich 1980), and (Vallado, et al. 2006).

3.2.3 TLE Analysis

In the previous section, the five General Perturbation theory sets were examined and the theory of choice was picked: SGP-4/SDP-4. In order for any system requirements for designing a new sensor to be generated, it is recommended to understand as to what element(s) can be improved upon the most and their behavior. To do this, the errors that result between propagating one Keplerian element to the next-generated one are examined. The format of TLEs are defined in *Spacetrack Report No. 3* (Hoots and Roehrich 1980) and *An Overview on Orbit Determination Techniques for TLE Generation* (Schattenberg 2017).

To do this, the errors that result in propagated measurements to those values released on the subsequent TLEs using the propagator of choice are investigated. In other words, the orbital elements from TLE #1 are taken and propagated to the timestamp in TLE #2 using the chosen propagator. The positional difference is the magnitude of the distance of the Cartesian Coordinates of the satellite using TLE#1 at the timestamp of TLE #2 and the same satellite's Cartesian Coordinates from TLE #2. These results are then saved for analysis.

Using the below TLEs as an example, the time interval between the two TLEs (one-minute shy of eight hours), and the chosen propagator, Table 3-1 can be generated.

TLE #1

```
1 32789U 08021G   17051.91214729 +.00002670 +00000-0 +19514-3 0  9997
2 32789 097.5746 112.5388 0013982 134.6845 225.5523 15.04408841479280
```

TLE #2

```
1 32789U 08021G   17052.24471266  .00002800  00000-0  20443-3 0  9993
2 32789  97.5747 112.8647 0014011 133.6142 226.6249 15.04411181479430
```

Table 3-1. TLE Propagation of the Slow Variables. The slow variables in "TLE #1" are propagated to the timestamp at TLE#2 (17052.24471266) using SGP-4. The relative error is the percent error between "#1 at #2" and "TLE #2."

	TLE #1	#1 At #2	TLE #2	Relative Error	
SMA [km]:	6931.45	6936.07	6931.45	4.62	0.07%
Eccen. [-]:	0.0014	0.0022	0.0014	0.0008	57.62%
Incl. [deg]:	97.5746	97.5695	97.5747	0.0052	0.01%
RAAN [deg]:	112.540	112.865	112.865	0.0004	0.00%

What can be seen for these two particular TLEs, is that the slow orbital elements that experience the largest change is in the inclination of the satellite, followed by the semi-major axis, and the least amount of change in the right ascension of the ascending node (RAAN). However, two points can be argued here: the errors are dependent upon the size of the satellite (presented below) and in how close a value is to zero. For the latter, assuming a near-circular orbit with an eccentricity close to zero, any small change in the eccentricity will result in a large relative error. This seems to be the case for the eccentricity presented above.

With respect to the size of the satellite, 29 different satellites with a geometrical radar cross section ranging from 48 square centimeters to 3.935 square meters for a year's worth of TLEs were analyzed. With this information, not only can the positional differences of TLE #1 at the timestamp in TLE#2 be calculated, but also the change in the individual orbital elements as a function of the geometrical radar cross section as well. The results for the positional differences are presented in Figure 3-2 and changes in TLE's are presented in Figure 3-3 through Figure 3-6. More information concerning these results can be found in *Long-Term Performance Analysis of NORAD Two-Line Elements for CubeSats and PocketQubes* (Speretta, Sundaramoorthy and Gill 2017).

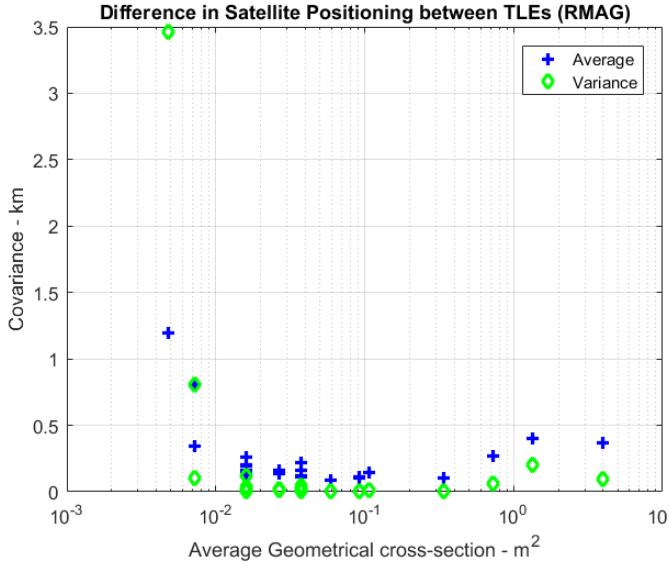

Figure 3-2. Difference in Satellite Positioning between TLEs. More information on the creation of this graph can be found in *Long-term performance analysis of NORAD Two-Line Elements* (Speretta, Sundaramoorthy and Gill 2017).

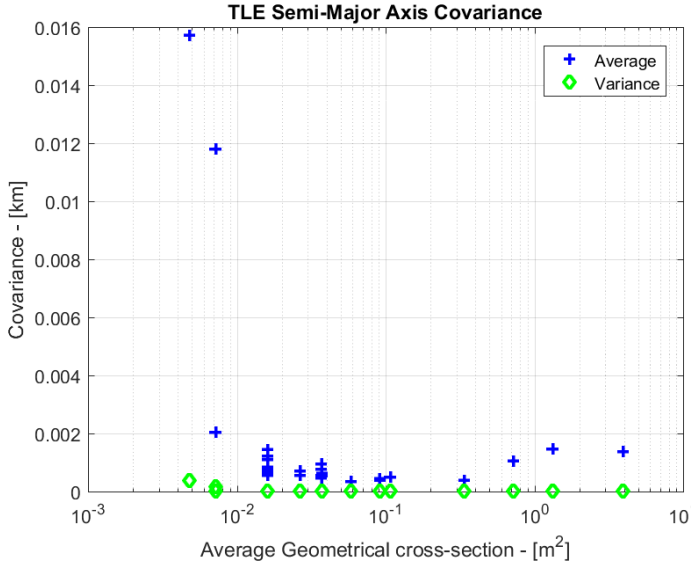

Figure 3-3. Difference in Semi-Major Axis between TLEs. These values were calculated using the same method and satellites as referenced in Figure 3-2 for a years-worth of TLEs.

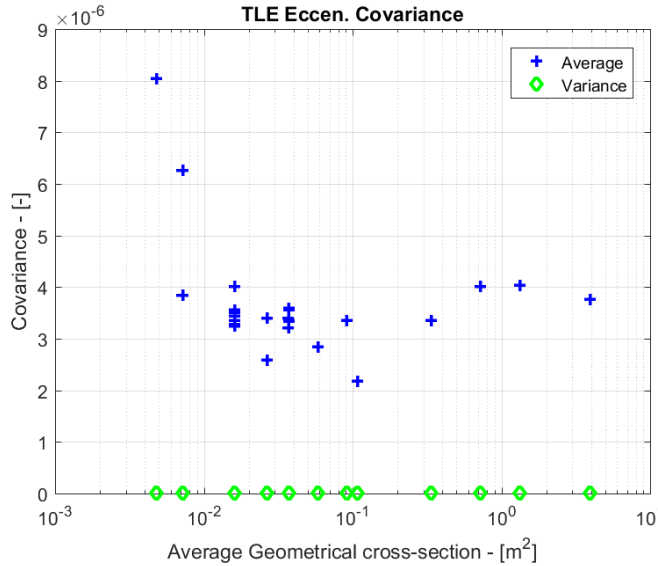

Figure 3-4. Difference in Eccentricity between TLEs. These values were calculated using the same method and satellites as referenced in Figure 3-2 for a years-worth of TLEs.

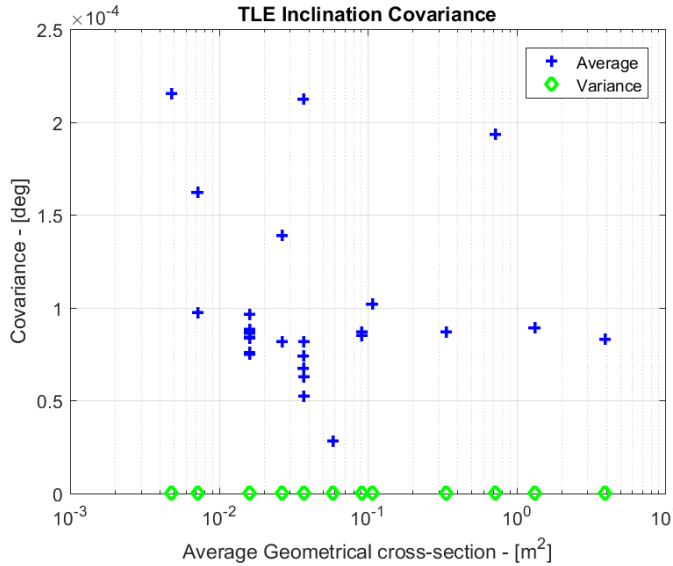

Figure 3-5. Difference in Inclination between TLEs. These values were calculated using the same method and satellites as referenced in Figure 3-2 for a years-worth of TLEs.

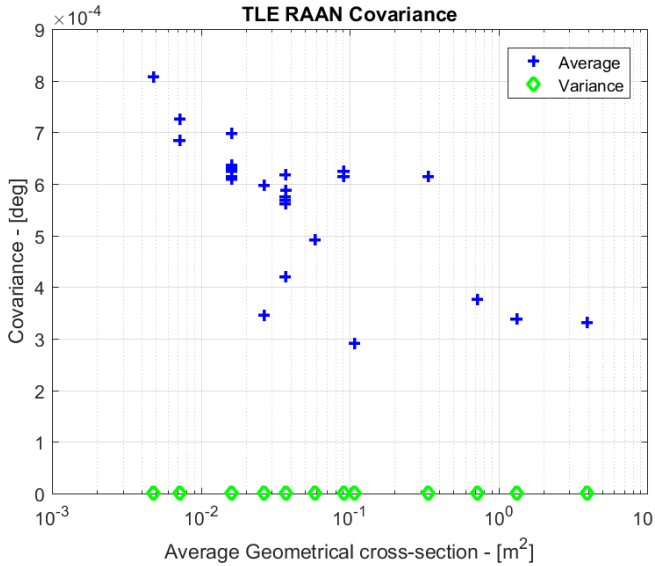

Figure 3-6. Difference in RAAN between TLEs. These values were calculated using the same method and satellites as referenced in Figure 3-2 for a years-worth of TLEs.

From examining Figure 3-3 through Figure 3-6, it can be seen that the calculated covariance as a function of the average geometrical cross-section for the eccentricity, inclination and right ascension of the ascending node are all much lower than that of the semi-major axis. What this result means is that by propagating the orbital elements from one timestamp on a TLE to the timestamp on the next-available TLE, the semi-major axis still experiences the largest change. Therefore, since the research objective deals with trying to calculate a better positioning estimate of satellites, this report will focus on improving the orbital element with the largest covariance, the semi-major axis.

3.2.4 Julian Day

The Julian Day is a continuous count in the number of days and fractional part of days that have elapsed since the beginning of the year -4712. By convention, the Julian Day begins at noon, 12^h UTC, at Greenwich. The Julian Day is useful in calculating astronomical phenomena because it does not include any leap days or leap seconds, and because it allows for a fast way to calculate the amount of time that has elapsed between

the two different time intervals. This means that the Julian Day progresses linear in time. For these reasons, all dates used in calculations for this thesis were immediately converted to their respective Julian Date using the algorithm presented in *Astronomical Algorithms* (Meeus 2009). This algorithm is presented below.

The required Julian Day is calculated using the following equation:

$$JD = INT\big(365.25(Y + 4716)\big) + INT\big(30.6001(M + 1)\big) + D + B - 1524.5 \quad \text{3-1}$$

In this equation, INT represents the integer part of the calculated number. Variables *Y*, *M*, and *D*, are defined as the year, month, and day (including the *fractional part* of a day), respectively. Dependent on the month, *Y* and *M* may be modified by the following rule:

$$\left.\begin{matrix} Y = Y \\ M = M \end{matrix} \middle| \; M > 2 \right\} \qquad \left.\begin{matrix} Y = Y - 1 \\ M = M + 12 \end{matrix} \middle| \; M = 1 \; or \; 2 \right\} \quad \text{3-2}$$

Thus, if the month for the date of interest is *January* or *February*, the month is treated as a date after the end of *December* from the previous year.

The variable *B* in Equation 3-1 is expressed as a function of the year.

$$A = INT\left(\frac{Y}{100}\right) \quad \text{3-3}$$

$$B = 2 - A + INT\left(\frac{A}{4}\right) \quad \text{3-4}$$

As also stated in *Astronomical Algorithms*, the number 30.6 is expressed with zeros followed by a number. This fix comes from how computers interpret real numbers written in binary. By using 30.6 instead of 30.6001, a calculated number *might* give a result of 396.9998, whose inte-

ger part is 396 instead of 397. This small difference would ultimately result in an incorrect Julian Date.

3.2.5 The Mean Sidereal Time at Greenwich

Sidereal time is the measure of time defined by the motion of the ascending node of the ecliptic on the equator, usually expressed as an hour angle. *Greenwich Mean Sidereal Time* (GMST) is useful in coordinate transformations between an *Earth-Centered, Earth-Fixed* (ECEF) and an *Earth-Centered Inertial* (ECI) frame. Greenwich Mean Sidereal Time, can be calculated in two different ways: via the Sidereal Time at Greenwich at 0^h UT of a given date, or via the Sidereal Time at Greenwich at any instant of UT. For this report, the latter of the two was chosen since in converting between two coordinate systems at any given instant of UT. The following algorithm is used to calculate the GMST for any instant of UT.

First, the Julian Day of interest, as defined in Section 3.2.4, is calculated. Then, the Julian Century for the J2000 stand epoch, T, is found using Equation 3-5.

$$T = \frac{JD - 2451545.0}{36525} \tag{3-5}$$

Since the Julian Day is the day corresponding to a particular time instance in UT, the Greenwich Mean Sidereal Time, θ_0, can be determined with the following equation:

$$\theta_0 = 280.460\,618\,37 + 360.985\,647\,366\,29(JD - 2451545.0) + 0.000\,387\,933T^2 - T^3/(387\,100\,00). \tag{3-6}$$

There is a high probability that the above Sidereal Time, expressed in degrees, will not fall between the interval [0,360). Thus, multiples of 360 degrees should be added or subtracted until θ_0 falls between this interval.

3.2.6 Coordinate System Conversions

Below, two different coordinate system transformations are presented. The first method allows for the conversion to-and-from an Earth-Centered, Earth-Fixed (ECEF) and an Earth Centered Inertial (ECI) reference frame. Both these reference frames are defined in *Fundamentals of Astrodynamics and Applications* (D. A. Vallado 2007). The second coordinate system transformation allows for the conversion from the geocentric equatorial position cartesian coordinates, as defined in *Fundamentals of Astrodynamics* (Bate, Mueller and White 1972, 55), to Keplerian elements.

3.2.6.1 EARTH-CENTERED, EARTH-FIXED TO EARTH-CENTERED INERTIAL

The positioning data for the satellites used in this analysis are defined in a rotating coordinate system, rather than SPG4's coordinate system, ECI. This means that in order to improve upon positioning estimates, all positioning vectors need to be converted into the same coordinate system before they can be compared.

In order to accomplish this transformation, four matrices are needed. These matrices are the procession matrix, D, nutation matrix, C, Sidereal Time matrix, B, and the polar motion matrix, A. This transformation is defined by the following set of equations (National Geospatial-Intelligence Agency n.d.):

$$\boldsymbol{R}_{ECI} = [ABCD]\boldsymbol{R}_{ECEF} \tag{3-7}$$

In Equation 3-7, $[ABCD]$ represents the four matrices as listed above. Matrix D represent the *precession* matrix and consists of three angles, ζ, z, and θ (not to be confused with GMST) and is defined by the equations below (Lieske 1978). The variable T is as previously defined in Section 3.2.5.

$$\zeta = 2306\overset{''}{.}2181\,T + 0\overset{''}{.}30188\,T^2 + 0\overset{''}{.}017998\,T^3 \tag{3-8}$$

$$z = 2306\overset{''}{.}2181\,T + 1\overset{''}{.}09468\,T^2 + 0\overset{''}{.}018203\,T^3 \tag{3-9}$$

$$\theta = 2004\overset{''}{.}3109\,T - 0\overset{''}{.}42665\,T^2 - 0\overset{''}{.}041833\,T^3 \tag{3-10}$$

$$D = R_z[-90 - z]R_x[\theta]R_z[90 - \zeta] \quad 3\text{-}11$$

Matrix C is the *nutation* matrix and "transforms coordinates from the mean inertial system of date to the true inertial system of date" (National Geospatial-Intelligence Agency n.d., A-6). This matrix also is a rotation about three variables: the true obliquity of ecliptic, ε, the nutation in longitude, $\measuredangle\psi$, and the mean obliquity of ecliptic, $\overline{\varepsilon}$.

$$\epsilon = \overline{\epsilon} + \Delta\epsilon \quad 3\text{-}12$$

$$\overline{\epsilon} = 84381''.448 - 46''.8150T - 0''.00059\,T^2 + 0''.001813\,T^3 \quad 3\text{-}13$$

$$C = R_x[-\epsilon]R_z[-\Delta\psi]R_x[\overline{\epsilon}] \quad 3\text{-}14$$

In Equation 3-12, $\measuredangle\varepsilon$ is the *nutation in obliquity* and $\measuredangle\psi$ in Equation 3-14 is the *nutation in longitude*. The method in calculating these variables can be found in Jean Meeus' *Astronomical Algorithms* (Meeus 2009, 143-148).

Matrix B represents the *sidereal time* matrix and consists of one rotation about the z-axis about, Λ, "the longitude of the zero meridian from the true vernal equinox of date" (National Geospatial-Intelligence Agency n.d.). According to the NGIA paper, Λ, is a function of GMST at 0^h UT1, the *Apparent Minus Mean* Sidereal Time, $\measuredangle H$, Earth's rotation rate in a precessing frame, ω^*, the time within a day, t, and the difference between UTC and UT1, $\measuredangle t$.

$$\Lambda = H_0 + \Delta H + \omega^*(t - \Delta t) \quad 3\text{-}15$$

$$B = R_z[\Lambda] \quad 3\text{-}16$$

Matrix A represents the *polar motion* matrix. In other words, this is the wobble of Earth's rotational axis relative to its crust. This matrix is the final conversion and brings the transformed coordinates into a mean Earth-Centered, Earth-Fixed system. This matrix consists of two rota-

tions: one about x_p and another about y_p. The values for x_p and y_p were obtained from Standard EOP data files from the *International Earth Rotation and Reference Systems Service* (International Earth Rotation and Reference Systems Service 2013). These variables are defined as the "angular displacement of Earth's rotation axis from the mean terrestrial pole" as measured 1) "along the zero meridian (positive south)," and 2) "normal the zero meridian (positive west)" (National Geospatial-Intelligence Agency n.d., A-28).

$$A = R_y[-x_p]R_x[-y_p] \tag{3-17}$$

With Equation 3-17, the angles of x_p and y_p are small and it's "technically permissible" to use small-angle approximations [sic]. A summary of all the equations needed to calculate the rotation matrix between an ECI and ECEF frame can be found in the National Geospatial-Intelligence Agency paper titled *Transformation of ECI (CIS, Epoch J2000.0) Coordinates to WGS 84 (CTS, ECEF) Coordinates* on pages A-29 and A-30. These angles, were obtained from the IERS datacenter for the Julian Date of interest (International Earth Rotation and Reference Systems Service 2013).

Due to effects which can be considered negligible, i.e. the nutation in longitude, the precession of Earth taking approximately 26,000 years, and maximum amplitude in the polar motion of about nine meters in any direction (D. A. Vallado 2007, 215) (Montenbruck and Gill 2000, 183), matrix *[ABCD]* reduces to only matrix B. This matrix is expanded in Equation 3-16, and presented below.

$$\boldsymbol{R}_{ECI} = \begin{bmatrix} \cos\Lambda & \sin\Lambda & 0 \\ -\sin\Lambda & \cos\Lambda & 0 \\ 0 & 0 & 1 \end{bmatrix} \boldsymbol{R}_{ECEF} \tag{3-18}$$

In *Fundamentals of Astrodynamics and Applications*, David A. Vallado specifically states, "less accurate calculations sometimes use just the transformation for sidereal time. This option is often exercised and seldom documented!" (D. A. Vallado 2007, 233). However, in order to be thor-

ough in calculations, this process is documented in this report and all matrices listed in Equation 3-7 were included in transforming all coordinates between ECI and ECEF.

3.2.6.2 CARTESIAN TO KEPLERIAN COORDINATES

The function for converting cartesian coordinates into Keplerian elements used within this report was developed by David Vallado and is defined in *Fundamentals of Astrodynamics and Applications* (D. A. Vallado 2007). His method takes the geocentric equatorial position and velocity vectors from truth data and converts them into the six classical orbital elements. These classical orbital elements are the

1. Semi-major axis, a,
2. Eccentricity, e,
3. Inclination, i,
4. Right ascension of the ascending node, Ω,
5. Argument of perigee, ω, and the
6. True anomaly, υ, or mean anomaly, M.

Of these six Keplerian elements, the first two (a and e) set the shape and size of the orbit. The next two elements (i and Ω) define the plane of the orbit. The argument of perigee defines the rotation of the semi-major axis with respect to Earth's equatorial plane. And finally, the true or mean anomaly describes the position of the satellite in its orbit at a specified time. With these six classical Keplerian elements and the propagator presented in Section 3.2.2, the satellite's position and Keplerian elements can be calculated at any specific time in the past, present and/or future.

The conversion from the geocentric equatorial position cartesian coordinates can be found in a plethora of literature, thus, to add to this plethora of literature, the method found in *Fundamentals of Astrodynamics* (Bate, Mueller and White 1972, 58-71), *Fundamentals of Astrodynamics and Applications* (D. A. Vallado 2007) and in other sources as well, is presented below.

First, three fundamental vectors need to be calculated. These are the *angular momentum vector*, $\boldsymbol{h}$, the *node vector*, $\boldsymbol{n}$, and the *eccentricity vector*, $\boldsymbol{e}$. These three vectors are computed via equations 3-19, 3-20, and 3-21.

Non-bolded variables represent the magnitude of the vector and **bolded** variables represent the vector of their non-bolded counterpart. In the following expressions, μ represents the gravitational parameter of Earth.

$$\boldsymbol{h} = \boldsymbol{r} \times \boldsymbol{v} \tag{3-19}$$

$$\boldsymbol{n} = \begin{vmatrix} i & j & k \\ 0 & 0 & 1 \\ h_i & h_j & h_k \end{vmatrix} \tag{3-20}$$

$$\boldsymbol{e} = \frac{1}{\mu}\left[\left(v^2 - \frac{\mu}{r}\right)\boldsymbol{r} - (\boldsymbol{r} \cdot \boldsymbol{v})\boldsymbol{v}\right] \tag{3-21}$$

After calculating the above vectors, the first step is to calculate the specific mechanical energy, ε, and the semi-major axis, a:

$$\epsilon = \frac{v^2}{2} - \frac{\mu}{r} \tag{3-22}$$

$$a = -\frac{\mu}{2\epsilon} \tag{3-23}$$

Using the value obtained in Equation 3-19, the orbital *inclination*, i, is defined as:

$$\cos i = \frac{h_k}{h} \tag{3-24}$$

Then, calculate the *right ascension of the ascending node*, Ω, by means of the following equation:

$$\cos \Omega = \frac{n_i}{n} \tag{3-25}$$

Next, if n_j is greater than zero, the sign for Ω is left unchanged. Otherwise, the value of Ω is 2π minus Ω.

Next the argument of perigee, ω, and the true anomaly, ν, are found with the following equations:

$$\cos\omega = \frac{\boldsymbol{n}\cdot\boldsymbol{e}}{n\,e} \tag{3-26}$$

$$\cos\nu = \frac{\boldsymbol{e}\cdot\boldsymbol{r}}{e\,r} \tag{3-27}$$

And then, once again, for the argument of perigee, if e_k is less than zero, the sign for ω is negated. Similarly, with the true anomaly: if $\boldsymbol{r}\cdot\boldsymbol{v}$ is less than zero, the sign for ν is negated.

Finally, the *mean anomaly*, M, is found first by solving for the *eccentric anomaly*, E, in Equation 3-28 and then for M in Equation 3-29:

$$\tan\frac{E}{2} = \tan\frac{\nu}{2}\sqrt{\frac{1-e}{1+e}} \tag{3-28}$$

$$M = E - e\sin E \tag{3-29}$$

3.2.7 Gibbs Method

J. W. Gibbs developed this method in the mid-1800's as a "method for determining an orbit from three position vectors" using a pure geometrical and vectoral approach (Bate, Mueller and White 1972, 109). The assumptions made in using this method are that the three position vectors are nonzero, coplanar, and represent *time-sequential* vectors (D. A. Vallado 2007, 450).

The reason why this method was chosen over other orbit determination methods to derive the velocity component is because it works with angles all the way down to about one degree and works with truth data that only has positioning information available. This method relies solely on vector analysis and therefore vectors that are most spaced out will yield better results and not suffer from numerical instability (D. A. Vallado 2007, 455). This method "appears to be foolproof in that there are no known special cases" where problems such as quadrant resolution

arise, and because it is a "very efficient [method] for use in a computer solution to problems of this type" (Bate, Mueller and White 1972, 114 & 116).

3.2.7.1 THE ALGORITHM

Gibbs Method is derived and further explained in *Fundamentals of Astrodynamics and Applications* (D. A. Vallado 2007) and *Fundamentals of Astrodynamics* (Bate, Mueller and White 1972); however, a shortened version is also presented here, since it serves as the backbone in analysis of shadow times, and because it is further explored in Section 3.2.7.2.

In short, Gibbs Method requires three coplanar position vectors $\boldsymbol{r_1}$, $\boldsymbol{r_2}$, and $\boldsymbol{r_3}$ obtained from time-sequential measurements by any technique. With these three vectors, three new vectors are formed: $\boldsymbol{D}$, $\boldsymbol{N}$, and $\boldsymbol{S}$.

$$\boldsymbol{D} = \boldsymbol{r_1} \times \boldsymbol{r_2} + \boldsymbol{r_2} \times \boldsymbol{r_3} + \boldsymbol{r_3} \times \boldsymbol{r_1} \tag{3-30}$$

$$\boldsymbol{N} = r_3\boldsymbol{r_1} \times \boldsymbol{r_2} + r_1\boldsymbol{r_2} \times \boldsymbol{r_3} + r_2\boldsymbol{r_3} \times \boldsymbol{r_1} \tag{3-31}$$

$$\boldsymbol{S} = (r_2 - r_3)\boldsymbol{r_1} + (r_3 - r_1)\boldsymbol{r_2} + (r_1 - r_2)\boldsymbol{r_3} \tag{3-32}$$

With the calculated $\boldsymbol{D}$, $\boldsymbol{N}$, and $\boldsymbol{S}$ vector, check that $D \neq 0$, $N \neq 0$, and $\boldsymbol{D} \cdot \boldsymbol{N} > 0$ to make sure that a possible two-body orbit exists. If this is true, calculate the vector and scalar, $\boldsymbol{B}$ and L, respectively.

$$\boldsymbol{B} = \boldsymbol{D} \times \boldsymbol{r_2} \tag{3-33}$$

$$L = \sqrt{\frac{\mu}{DN}} \tag{3-34}$$

Then calculate the vector $\boldsymbol{v_2}$.

$$\boldsymbol{v_2} = \frac{L}{r_2}\boldsymbol{B} + L\boldsymbol{S}. \tag{3-35}$$

With $\boldsymbol{r_2}$ and $\boldsymbol{v_2}$ found, the method described in Section 3.2.6.2 can be used to solve for the orbital elements.

3.2.7.2 CONCERNING LEO TRUTH DATA

Gibbs Method was also used for the truth data supplied by the Space Exploration Department at the Technical University of Delft. Their truth data *does* contain velocity vectors, however when comparing the calculated Keplerian elements to those found in a TLE, the calculated quantities using the supplied velocity vectors were not even close.

As an example, the following TLE

```
1 27391U 02012A   05001.17201054  .00002419  00000-0  78765-4 0  9996
2 27391 089.0240 219.2330 0015153 311.7148 048.2843 15.31318717155891
```

was propagated *nine* seconds forward in time to be at the same timestamp for the same satellite as the truth data supplied from the Technical University of Delft. This truth data is presented below. In it, the first line represents the timestamp, and the second and third line represent the x-, y-, and z-component in the position and velocity vectors, respectively.

```
                2005-01-01 05:07:50.000 UTC
-0.32532042611E+07 -0.29785614819E+07 -0.52481650339E+07
 0.42240655040E+04  0.40304214590E+04 -0.48929726660E+04
```

This truth data was converted from the ITRF to the ECI reference frame to be in the same frame of reference as the propagator's reference frame, and then converted to Keplerian elements. The results presented in Table 3-2 show that by using the true position and velocity vector for the truth data, the derived elements do not even closely resemble that of the TLE and the elements derived using Gibbs Method.

For this reason, Gibbs Method was also used to derive the Keplerian elements for the truth data supplied by the Space Exploration Department at the Technical University of Delft.

Table 3-2. A Comparison in Propagated Keplerian Elements between Truth Data and Gibbs Method.

Orbital Element	TLE +6 seconds	Using the Position and Velocity Vector from the Truth Data	Using Gibbs Method
a	6856.463 km	6944.968 km	6846.885 km
e	0.0014792	0.0237880	0.0001178
i	89.0247 deg	96.3434 deg	89.0443 deg
Ω	219.2330 deg	219.3663 deg	219.3017 deg
ω	358.8850 deg	54.8967 deg	327.8364 deg
M	1.6438 deg	307.8056 deg	32.6624 deg
ω+M	360.5288 deg	362.7023 deg	360.4988 deg

3.3 FIRST-ORDER APPROXIMATIONS OF SHADOW TIMES

Eclipses play a major role in being able to determine the satellite's heat balance, passive optical tracking, power, and orbit perturbation experienced with and without solar radiation pressure. By measuring the satellite's eclipse times, an approach using one of many numerical converging techniques can be applied in order to calculate a new semi-major axis that can be applied to TLEs to keep propagation errors lows. What makes eclipse times of particular interest is that they happen quite frequently, and thus corrections to TLEs can happen on a frequent basis.

An eclipse consists of three parts: the umbra, penumbra, and antumbra. These regions are defined in *Fundamentals of Astrodynamics and Applications* (D. A. Vallado 2007, 283-284,300-303) and are illustrated in Figure 3-7.

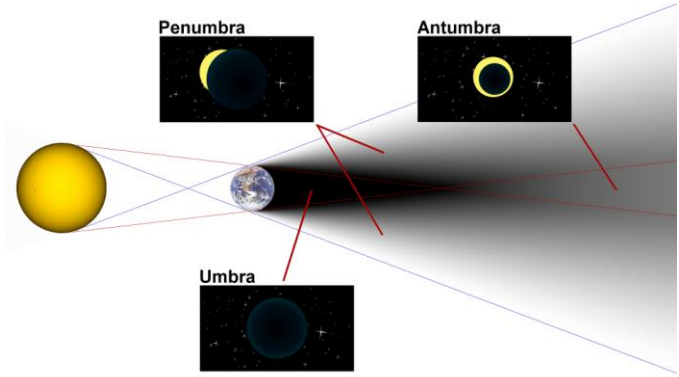

Figure 3-7. Three Parts of an Eclipses. Public domain image. A diagram of umbra, penumbra and antumbra in a two-body system. Copyright 2008 by Qarnos.

Two main methods exist for determining if a satellite is eclipsed. These two methods can be found in the report titled, *Eclipse Intervals for Satellites in Circular Orbit under the Effects of Earth's Oblateness and Solar Radiation Pressure* (Ismail, et al. 2015), and the book *Fundamentals of Astrodynamics and Applications* (D. A. Vallado 2007, 300-307). However, the latter of these two methods is more appropriate for numerical integration. Because of this and due to an apparent lack in literature existing for a non-numerical-integration-based solution for an *Earth Shadow Conical Shadow Model (ESCM)* similar to the *Earth Cylindrical Shadow Model (ECSM)*, a geometrical formulation was developed as a first-order approximation in calculating umbral eclipse times. These set of equations were also developed due to computation times in GMAT and SGP-4 taking more than a few seconds per run and the other methods having to run multiple times per iteration. The formulation of this method is presented in Section 3.3.2 and the performance of each model is shown in Table 3-5, Table 3-3, and Table 3-4.

3.3.1 Earth Cylindrical Shadow Model (ECSM)

The first method by Ismail, et al. details a solution in calculating eclipse times using five assumptions:

1. The Earth is modeled as a sphere with a radius equal to the mean radius of Earth.
2. There is no penumbra.
3. Refractions are negligible.
4. Due to small orbital periods, the synodic and sidereal periods are identical.
5. The satellite orbits Earth in a purely circular orbit.

This means that the shadow of Earth is modeled as a cylinder and incorporates part of the penumbra into the calculation of the umbral part of the eclipse (Figure 3-8).

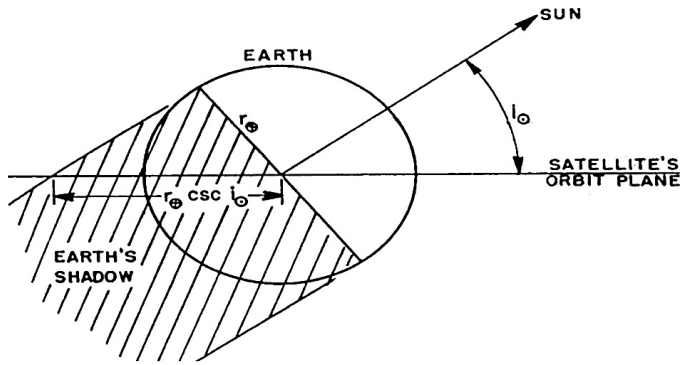

Figure 3-8. The Earth's Shadow with no Penumbra. Adapted from Eclipse Intervals for Satellites in Circular Orbit under the Effects of Earth's Oblateness and Solar Radiation Pressure by M. N. Ismail, et al., 2015, Copyright 2015 by Elsevier B.V.

Using the geometrical relations between the satellite's orbit plane and the plane of the sun, if magnitude of the satellite's radius vector, r, is less than $r_\oplus$ cosec($i_\odot$), then an eclipse will occur, and if r is greater than $r_\oplus$ cosec($i_\odot$), an eclipse will occur.

Using the above assumptions, Equation 3-36 and 3-37 result:

$$\tau_{circular} = \frac{P}{\pi}\operatorname{acos}\left(\frac{\sqrt{1-\left(\frac{R_{\oplus}}{r}\right)^2}}{\cos(i_{\odot})}\right). \quad 3\text{-}36$$

$$\sin(i_{\odot}) = \cos(i)\sin(\delta_{\odot}) + \sin(i)\cos(\delta_{\odot})\sin(\Omega - \alpha_{\odot}). \quad 3\text{-}37$$

In Equation 3-36, τ is the theoretical eclipse time for a satellite in a circular orbit, $i_{\odot}$ is the phase angle between the orbit plane of the satellite and the sun (Equation 3-37), $R_{\oplus}$ is the radius of Earth, r is the magnitude of the satellite's position vector, and P is the period of the satellite. In Equation 3-37, i is the inclination of the satellite, a and δ are the equatorial coordinates of the sun as calculated in *Astronomical Algorithms* (Meeus 2009, 163), and Ω and right ascension of the ascending node of the satellite. (Ismail, et al. 2015)

3.3.2 Earth Shadow Conical Model (ESCM)

Due to an apparent lack in literature existing for a non-propagator-based geometrical solution for an *Earth Shadow Conical Shadow Model*, an approach was developed as a first-order approximation for use in determining an initial guess for the semi-major axis of a satellite. This semi-major axis is then fed into the algorithm presented in Section 4.2.7 for shadow time analysis (Section 4.1).

This approach makes use of Equation 3-37 to calculate the phase angle between the satellite orbit plane and the Sun-Earth line. To arrive at the set of equations presented in this section, the following assumptions were made:

1. The satellite orbits about Earth in a pure circular orbit.
2. The Earth is modeled as a sphere with the radius equal to the mean radius of Earth.
3. There is no penumbra.
4. Refractions are negligible.

5. Due to small orbital periods, the synodic and sidereal periods are identical.

3.3.2.1 DETERMINING THE MAXIMUM ECLIPSE TIME

With all these assumptions being made, and making the additional assumption that the Sun, Earth, and satellite are all aligned in the same plane (i.e. β is equal to zero), the maximum amount of time a satellite spends in the umbral part of the Earth's shadow, T_{SH}, can be determined. This can be expressed as a percentage, θ/π, of the orbital period, P (Equation 3-39).

$$T_{SH} = \frac{\theta}{\pi} P \tag{3-38}$$

$$P^2 = \frac{4\pi^2 a^3}{\mu} \tag{3-39}$$

In Equation 3-39, a is the semi-major axis of the satellite, and μ is the gravitational parameter of Earth.

With this information, an expression can be developed for the angle, θ (as defined in Figure 3-10). To do this, a relation needs to be developed between the amount of arc from the satellites full orbit that falls within the umbral cone as a function of the semi-major axis of the satellite. The first step is to determine the value of ϱ_c, the slope of the umbral portion of Earth's shadow, and the distance between Earth and the location of c (Figure 3-9).

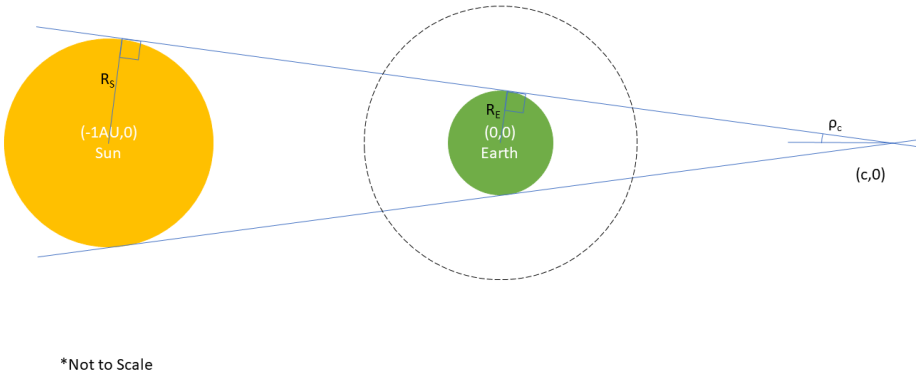

Figure 3-9. Eclipse Umbra Geometry. The orbit of the satellite is as viewed perpendicular to the orbit plane.

By using right triangles, the expression of ρ_c can be written as,

$$\tan \rho_c = \frac{R_S - R_E}{1AU\ [km]} \tag{3-40}$$

where R_S and R_E is the radius of the Sun and Earth, respectively. The distance between the Sun and the Earth is 1AU (*Astronomical Unit*) and is expressed in kilometers. The variable ρ_c is as previously defined in Figure 3-9.

The development for the expression of the location of c, the distance between the center of Earth and the apex of the shadow cone, is found in *Fundamentals of Astrodynamics and Applications* (D. A. Vallado 2007, 301-302). The resulting equation is as follows:

$$c = \frac{1AU[km]R_E}{R_S - R_E} \tag{3-41}$$

Next, by zooming into the Earth-Satellite frame geometrical relationships between Earth, Satellite, and the Umbra Cone Apex (Figure 3-10) are constructed.

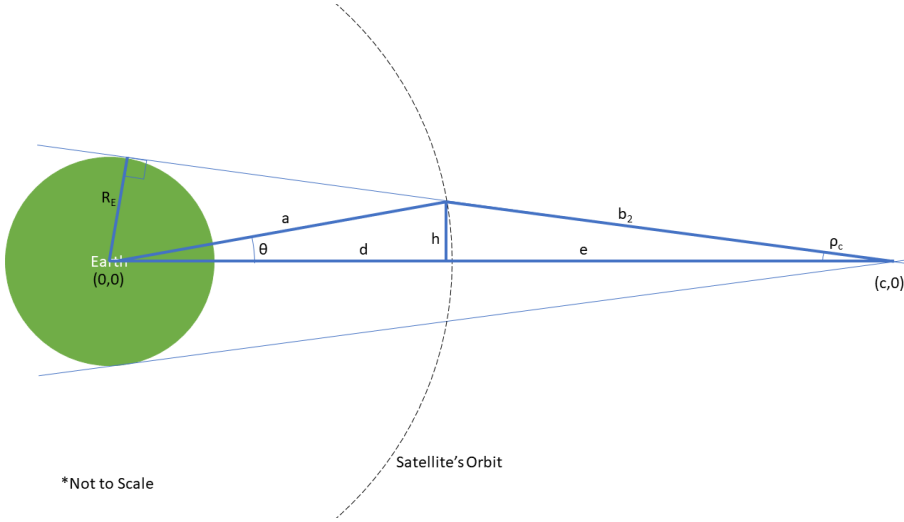

Figure 3-10. Umbra Conical Geometry. The orbit of the satellite is as viewed perpendicular to the orbit plane. In this figure, a is the semi-major axis of the satellite, R_E is the radius of the Earth, ρ_c is as previously defined, θ is one-half of the full angle that the satellite spends in the Earth's shadow, and b, d, e, and h are arbitrary letters for simplification of geometric expressions.

The first step in this procedure is to determine an expression for θ. This is accomplished by first dropping a vertical at the shadow-orbit intersection point and then summing up two geometrical relationships:

$$c = a\cos\theta + b\cos\rho_c \tag{3-42}$$

And by rearraigning the equation:

$$\theta = \cos^{-1}\left(\frac{c - b\cos\rho_c}{a}\right) \tag{3-43}$$

Realizing that all variables are known except b, an expression needs to be developed for this variable. Using the *Law of Cosines* between a, b_2, c, and ρ_c, the following equation is constructed:

$$a^2 = b_2^2 + c^2 - 2b_2 c \cos \rho_c \tag{3-44}$$

Next, this equation is written as a function of b_2:

$$b_2^2 + (-2c \cos \rho_c) b_2 + (c^2 - a^2) = 0 \tag{3-45}$$

The roots of this univariate function are

$$b = c \cos \rho_c \pm \sqrt{c^2 \cos^2 \rho_c - c^2 + a^2} \tag{3-46}$$

Since the distance of interest is the shorter distance, b_2 in Equation 3-46, the smaller of the two roots is used. Then, by substituting Equation 3-40 back into Equation 3-43, a final expression can be written for determining the angle θ (Equation 3-47), and finally the maximum time a satellite will spend in the umbral part of an eclipse (Equation 3-38).

$$\cos \theta = \frac{c - (c \cos \rho_c - \sqrt{(c \cos \rho_c)^2 - c^2 + a^2}) \cos \rho_c}{a} \tag{3-47}$$

3.3.2.2 ACCOUNTING FOR ORBIT PLANE OFFSETS

In order to account for the phase angle between the satellite and the Sun-Earth line, two methodologies were considered: a method using strictly planar trigonometry, and the other using spherical trigonometry. The first method used a series of right triangles to determine the degrees of arc of the orbit wherein the satellite would be in eclipse. The second method utilized one of *Napier's rules'* relationship for right spherical triangles.

From these two methods, the most straightforward approach was to apply *Napier's rules* for right spherical triangles due to the fact that a rela-

tionship can be formed between all three sides of the spherical triangle. This method is presented below.

To start, the value of θ presented in Equation 3-47 is only valid when the satellite, Earth, and Sun are all in the same orbital plane. When the satellite's orbit is outside of this plane, the value of θ in Equation 3-47 is no longer valid and the amount of arc that the satellite travels through is smaller. However, the general expression in Equation 3-38 still remains valid, but θ takes on a slightly different meaning (i.e. θ is expressed as a function of itself and β).

To start, this problem was visualized as a series of geometrical shapes. Namely, a sphere, to represent all possible orbits at a certain altitude, and a cone, to represent the umbral shadow of the Earth. In Figure 3-11, these two shapes are shown. The part that is of interest is the intersection point of the sphere and the cone. Any point inside this cone along the surface of the sphere represents all locations where the satellite is eclipsed.

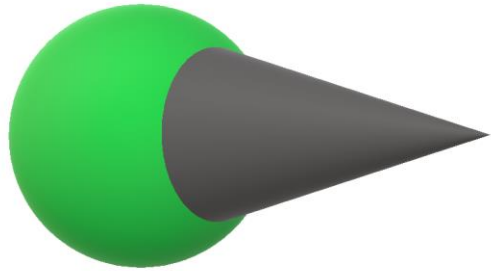

Figure 3-11. Satellite's Orbit Sphere and Umbral Cone. The green sphere represents a sphere with the radius equal to the orbital radius of the satellite, assuming a circular orbit. The grey cone represents the umbra shadow region. The Earth lies inside at the center of the green sphere. This figure is exaggerated and is not drawn to scale.

In order to analyze the arc that the satellite will fly inside the eclipse, a slice is taken at the intersection point of sphere and cone. This spherical cap represents the locations where the satellite is in eclipse. This cap is shown in Figure 3-12 as the thick black line. The blue line is the arc, θ, as defined in Equation 3-47. The angle β is the phase angle. This angle has the same arc angle as the equatorial line shown on the hemisphere. This is the black line connecting the red and blue line along the middle of the hemisphere.

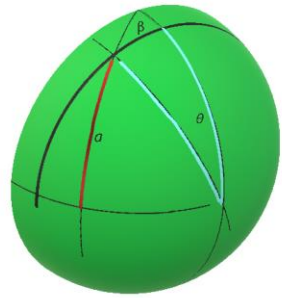

Figure 3-12. Satellite Orbits and Angles.

From Figure 3-12, the part of interest is in determining how many degrees of arc the satellite is flying along the red line (denoted by a in Equation 3-48). Recognizing that the angle made between the black equatorial line and the red phase angle line, a, from β, is 90-degrees, a simplified version of one of *Napier's rules* can be applied:

$$\cos a \cos \beta = \cos \theta \qquad 3\text{-}48$$

This allows for the calculation of arc a, for any phase angle. In this equation, when β is zero, a equals θ. This represents an orbit when the satellite, Earth, and Sun are all in the same plane. Furthermore, when β is equal to or greater than θ, a in Equation 3-48 equates to zero or an imag-

inary number (i.e. no eclipse is possible). This calculated value of c takes the place of θ in Equation 3-38 (Equation 3-49).

Therefore, all the information now exists for calculating a first-order approximation for the amount of time a satellite spends in eclipse given a shift in its phase angle. These equations are presented below with all variables as previously defined.

$$T_{SH} = \frac{a}{\pi} P \tag{3-49}$$

$$c = \frac{1AU[km]R_E}{R_S - R_E} \tag{3-50}$$

$$\cos\theta = \frac{c - (c\cos\rho_c - \sqrt{(c\cos\rho_c)^2 - c^2 + a^2})\cos\rho_c}{a} \tag{3-51}$$

$$\begin{aligned}\sin(\beta) &= \cos(i)\sin(\delta_\odot) \\ &+ \sin(i)\cos(\delta_\odot)\sin(\Omega - \alpha_\odot).\end{aligned} \tag{3-52}$$

3.3.3 A Comparison between the Two Models

Ismail's relation is fine for general "back of the envelope" calculations; however, as the semi-major axis of the satellite and phase angle increase, so do the errors (Figure 3-13 and Figure 3-14).

As an example, if a worst-case scenario is taken where the phase angle of the satellite equals zero degrees, i.e. the maximum amount of time a satellite will theoretically spend in an eclipse, the errors between the two models are less than five percent up to an *altitude* slightly greater than 30,000 kilometers (Figure 3-13). However, as the phase angle increases and moves away from the Earth-Sun plane, the two models start to diverge (Figure 3-14).

It should be noted that GMAT does not provide a way to explicitly define a phase angle. Due to this limitation, Figure 3-13 does not include shadow intervals calculated by GMAT; nonetheless, for a phase angle of zero degrees, both methods provide similar results. Table 3-5, Table 3-3,

and Table 3-4 show a comparison of calculated eclipse times (accounting for a phase angle) between all shadow models for the LEO Satellites GOCE, CHAMP, and GRACE-A, respectively.

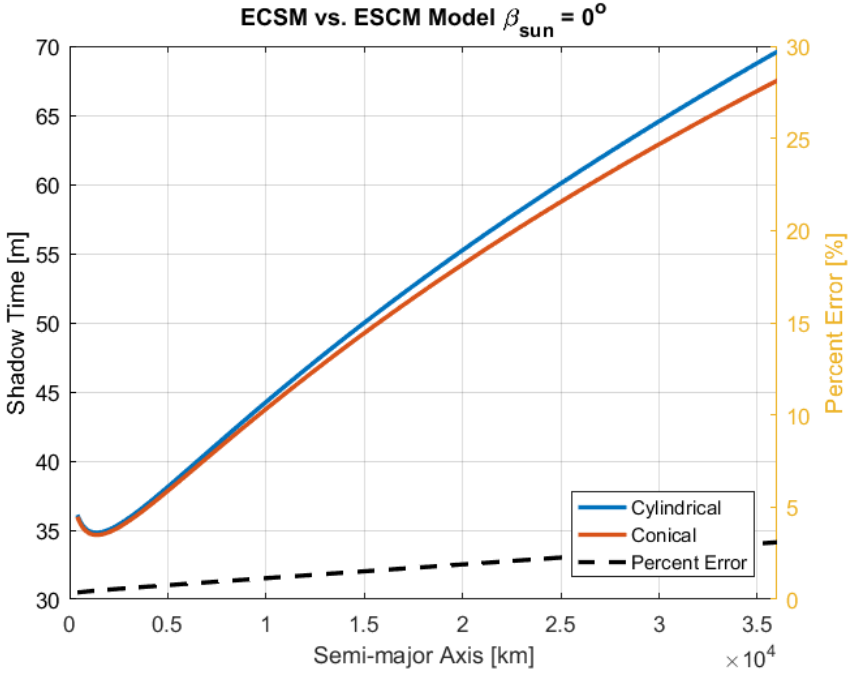

Figure 3-13. Earth Shadow Models for a Satellite in the Earth-Sun-Line Plane.

Table 3-3. Shadow Model Comparison for GOCE. This table was generated from the TLE presented in Appendix D.

Model	Eclipse Times [sec]	Computation Time [sec]
ECSM	2058.74	0.013010
ESCM	1814.50	0.012665
SGP-4	1799.31	1.260001
GMAT	1778.42	4.036157
Real Data	1803.08	3.456365

Table 3-4. Shadow Model Comparison for CHAMP. This table was generated from the TLE presented in Appendix D.

Model	Eclipse Times [sec]	Computation Time [sec]
ECSM	2111.85	0.012736
ESCM	2030.00	0.024441
SGP-4	2022.95	12.823254
GMAT	2013.30	3.958466
Real Data	2023.64	3.885953

Table 3-5. Shadow Model Comparison for GRACE-A. This table was generated from the TLE presented in Appendix D.

Model	Eclipse Times [sec]	Computation Time [sec]
ECSM	1915.63	0.015862
ESCM	1554.50	0.010652
SGP-4	1518.08	30.564843
GMAT	1544.89	4.137995
Real Data	1520.63	3.553288

Furthermore, in comparing numerical simulations of LEO satellites using NASA's *General Mission Analysis Tool* (GMAT) (Section 4.1) with a cylindrical shadow model, the satellite can be inside the penumbra part of an eclipse on ingress and egress for about 12 seconds each. These simplifications mean that the theoretical umbral eclipse time of the satellite can be off by slightly less than half-a-minute. With this information and by consulting the data used to generate these graphs, it can be seen that this can create a positioning error offset in the semi-major axis of about 130 kilometers for a satellite flying at an altitude of 450 kilometers and of about 400 kilometers for a satellite at an altitude of 25,000 kilometers.

Therefore, a solution was sought after that could distinguish between the penumbral and umbral part of an eclipse while keeping calculated eclipse times as close to the real values as possible. However, due to approximate-nature of the methods presented above, the conical method was used initially used as an economical method in analyzing shadow

times. This method formed the basis of an initial estimate in developing a search space used in finding a more-exact-solution using SGP-4.

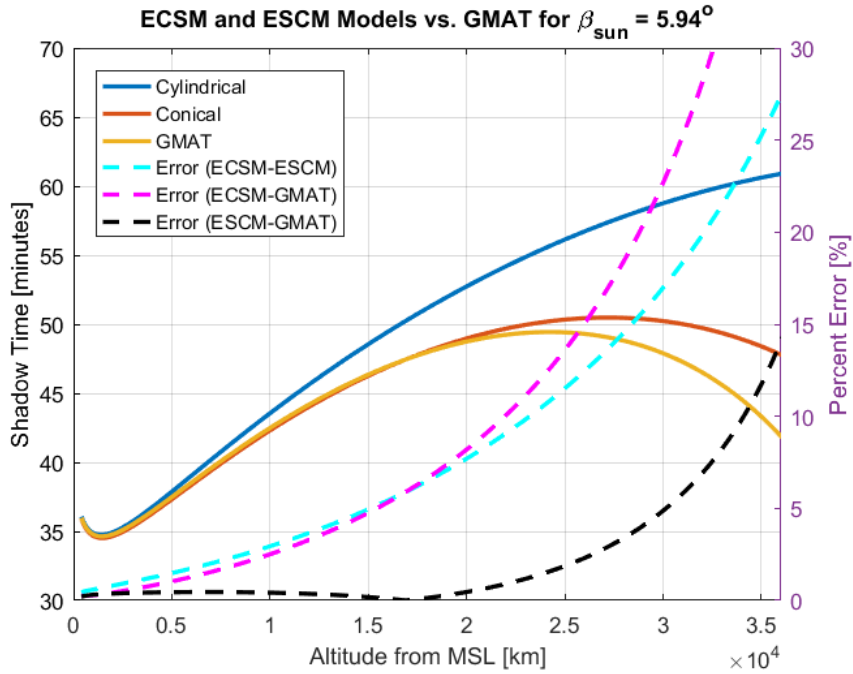

Figure 3-14. Earth Shadow Models Including a Phase Angle.

Thus, what can be concluded is that the conical method produces shadow times much faster than GMAT or SGP-4 that still closely resemble the true shadow time and thus can be used as a first-order approximation method in investigating the research objective and answering the research questions. Furthermore, what the ESCM shows is that it is advisable to use an Earth Shadow Conical Model for calculating theoretical eclipse times rather than using a cylindrical approximation.

4 Simulation Setup

"Equipped with his five senses man explores the universe around him and calls the adventure Science."

Edwin Hubble

This chapter combines the theory presented in Chapter 3 in order to analyze eclipse times of satellites. The data generated in this chapter is ultimately used to answer the research questions and to provide an answer to the research objective in Section 1.2.

In this chapter, GMAT is presented as one more tool for analysis since it can also be used as a stand-alone program for analyzing eclipse times. How this program was configured is explained in Section 4.1 as well as a comparison with the SGP-4 propagator. Ultimately, it was decided to use SGP-4 over GMAT for the reasons presented in Section 3.2.2, it provided more flexibility with integration into MATLAB, and because there is no streamlined way to use GMAT as a function inside of MATLAB. The implementation of SGP-4 into analysis and the MATLAB script is explained in Section 4.2

4.1 GENERAL MISSION ANALYSIS TOOL

The fundamental role of GMAT is to propagate and simulate the orbital dynamics of a spacecraft. According to Goddard Space Flight Center, "GMAT is an open source, platform independent trajectory optimization and design system designed to model and optimize spacecraft trajectories in flight regimes ranging from low Earth orbit to lunar applications, interplanetary trajectories, and other deep space missions" (Goddard Space Flight Center 2015). The information that can be obtained from simulating spacecraft orbits can be used in just about all parts of space mission analysis. This ranges from knowing when a spacecraft will fly overhead to numerically converging to a solution to determine precise thruster firing times and durations to send a spacecraft into interplanetary space.

This section is a condensed version of part of NASA's GMAT Manual (National Aeronautics and Space Administration 2017) and is written here as a tutorial in the same style on how GMAT was implemented for obtaining eclipse time intervals that were used as truth data in Section 4.2.5 for developing requirements for an eclipse sensor. Hopefully, this section also has the added benefit of teaching the reader the fundamental basics of GMAT and in obtaining numerical results about the orbit of a satellite. This section is broken up into the following steps with each one being explained in more detail in their respective parts:

1. Configure a **Spacecraft** and define its epoch and orbital elements.
2. Configure a **Propagator**.
3. Configure GMAT for **Event Locators**.
4. Add and configure an **EclipseLocator** to report eclipses.
5. Modify the **Propagate** command to propagate the spacecraft for the time duration of interest.
6. **Run** the GMAT mission and analyze the results.

4.1.1 Configure a Spacecraft

In this section, the spacecraft's initial epoch as well as import the orbital elements from the spacecraft's respective TLE will be configured. To start, GMAT will need to be open with the default mission loaded. To start a new mission, click on *File* → *New* → *Mission (CTRL + N)*.

4.1.1.1 RENAMING A SPACECRAFT

In the event that more satellites will be monitored at the same time, it is useful to rename the spacecraft in order to keep track of all the satellites. This can be accomplished by performing the following:

1. In the resources panel, click on **DefaultSC** and press **F2**.
2. Type in the name of the Satellite. In Figure 4-1, the spacecraft is named *G01*.
3. Click **OK**.

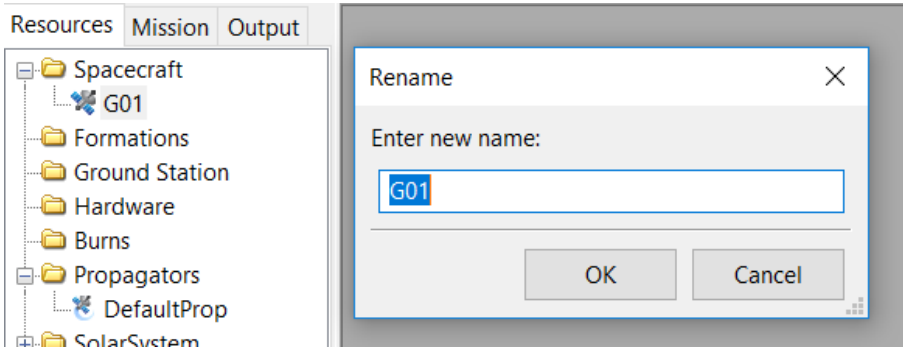

Figure 4-1. Renaming a Spacecraft.

4.1.1.2 SETTING THE EPOCH AND KEPLERIAN ELEMENTS OF THE SPACECRAFT

1. In the **Resources** panel, double-click on the recently-named satellite, and select the **Orbit** tab.
2. Drop down the **Epoch Format** list and select **UTCGregorian**.
3. In the **Epoch** field, type in the time that is valid for the respective orbital elements. The TLE has a different format and must be converted to its equivalent Gregorian Date. For this conversion and for the definition of TLEs, please consult Space Track Report #3 (Hoots and Roehrich 1980).
4. Drop down the **State Type** list and select **Keplerian**. The interactive boxes on the right-hand side will switch over to the Keplerian elements.
5. For the time of interest that was entered in step 3, fill in the orbital elements that appear on the TLE into their respective spot.

In this example, Table 4-1 lists the values that were used for this example.

Table 4-1. Satellite Orbit State Values. This table was generated using the following Two-Line Element for G01:

```
1 37753U 11036A   17203.54744446 -.00000040 +00000-0 +00000-0 0  9992
2 37753 055.4617 099.3649 0067763 032.0166 287.4387 02.00562478044058
```

Field	Value
SMA	P = 2.0056247804; SMA = 26501.98867846946
ECC	0.0067763
INC	55.4617
RAAN	99.3649
AOP	32.0166
TA	M = 287.4387; ν = 253.30398

6. The window should now look like Figure 4-2.Click on **Apply**, **OK**, and **Save** the document.

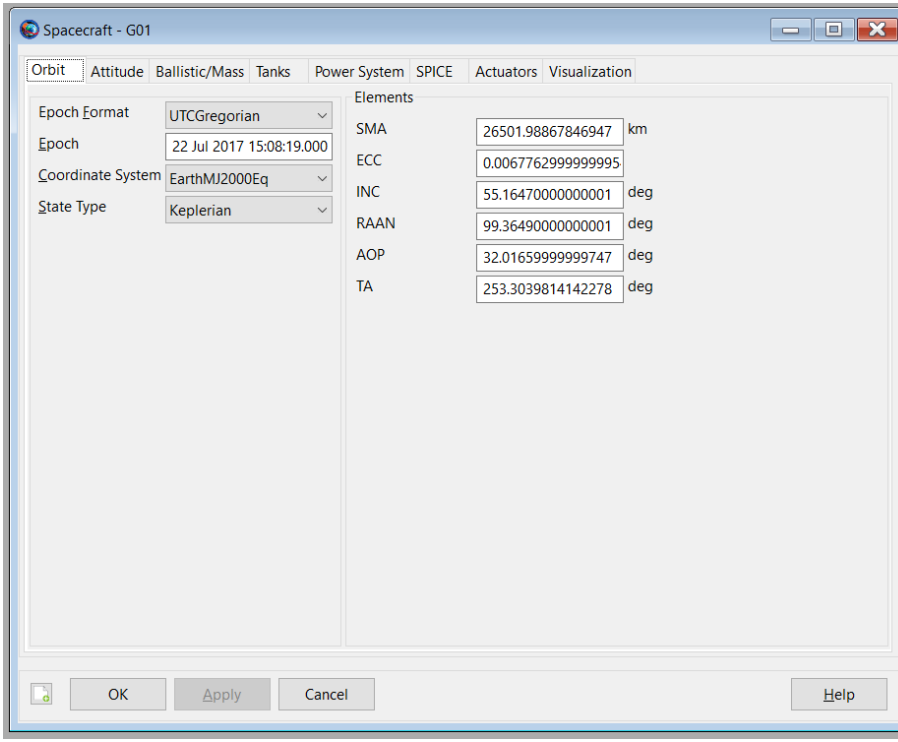

Figure 4-2. Completed Spacecraft State.

4.1.2 Numerical Propagator Configuration

For analysis of eclipse times and to account for many different forces acting upon a satellite, the following models and perturbations were taken into account for numerical propagation:

- Earth 10x10 Spherical Harmonic Model
- Jacchia-Roberts Atmospheric Model
- Solar Radiation Pressure, and
- Perturbations due to the Sun and Moon.

4.1.2.1 CONFIGURATING THE PROPAGATOR

1. In the **Resources** panel, double-click on **DefaultProp**.
2. Under the **Integrator** panel, drop-down the Integrator **Type** and select **PrinceDormand78**. According to the GMAT User Manual, this integrator is "the best all-purpose integrator in GMAT."

This integrator is an adaptive eighth-order Runge-Kutta integrator with seventh-order error control. (National Aeronautics and Space Administration 2017, 446)

3. Change the integrator's **Min Step Size** to **0**. By changing this value, the adaptive-part of the integrator is able to fully control the step size to assure the highest-possible accuracy.
4. Under **Force Model → Primary Body → Gravity**, change the **Degree** and **Order** to **10**. This assures that the Earth 10x10 Spherical Harmonic Model is going to be used.
5. Change the **Atmosphere Model** to **JacchiaRoberts**.
6. Click **Select** next to the **Point Masses** box and move **Luna** and **Sun** from the **Available Bodies** to the **Selected Bodies**.
7. Click on **OK** to close this dialog box.
8. Back on the previous menu, tick the box next to **Solar Radiation Pressure** and select **Spherical** for the **SRP Model**.
9. Click on **Apply**, **OK**, and **Save** the document.

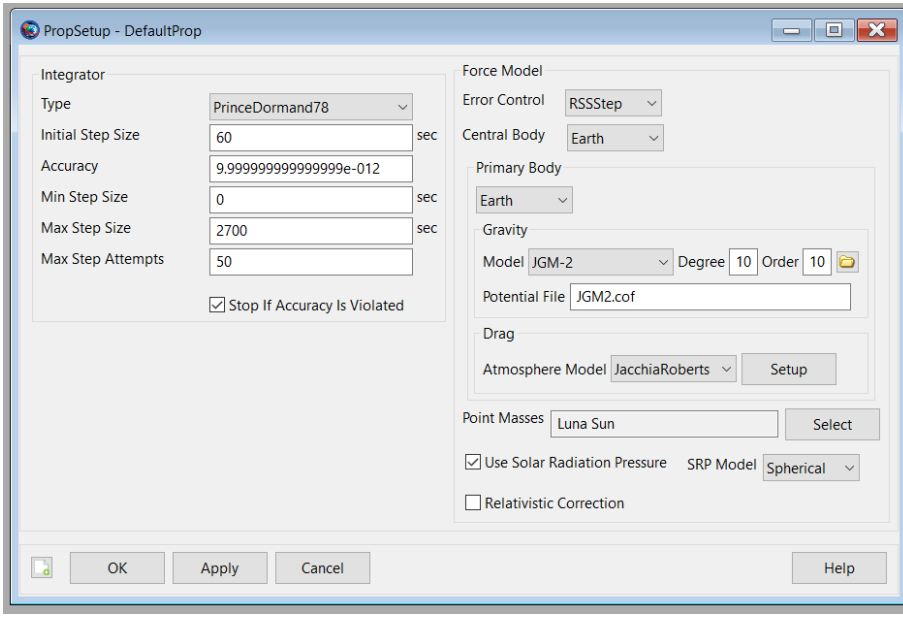

Figure 4-3. Propagator Configuration.

4.1.2.2 CONFIGURATING THE PROPAGATE COMMAND

Before running the designed mission, GMAT needs to know at least one condition to be satisfied in order for the integrator to stop running and compute the results. This value was set for two days into the future from the epoch specified on the TLE.

1. In the **Mission** panel, double-click on **Propagate1**.
2. Under **Stopping Conditions**, click on "…" next to **Parameter**. This will open the **ParameterSelectDialog** box.
3. Under **Object List** select the previously-named-satellite, if not already selected.
4. Move all the **Selected Value(s)** over to the **Object Properties** list. This will disable these parameters for the stopping conditions.
5. In the **Object Properties** box, double-click on **ElapsedDays** to move it over to the **Selected Value(s)** list. The window should now look like

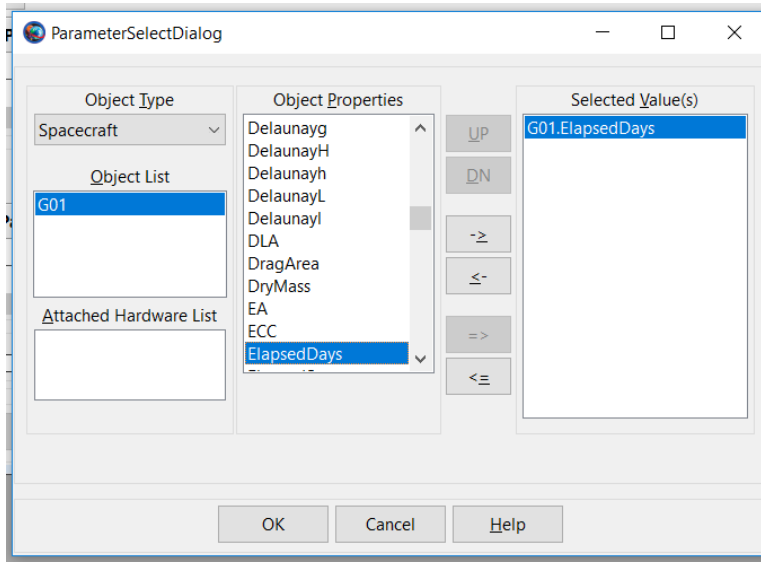

Figure 4-4. ParameterSelectDialog Configuration.

6. Click on **OK**.

7. Under **Stopping Conditions → Condition**, type in the number of days the orbit will be propagated. The screen should now resemble Figure 4-5.
8. Click on **OK**, and **Save** the document.

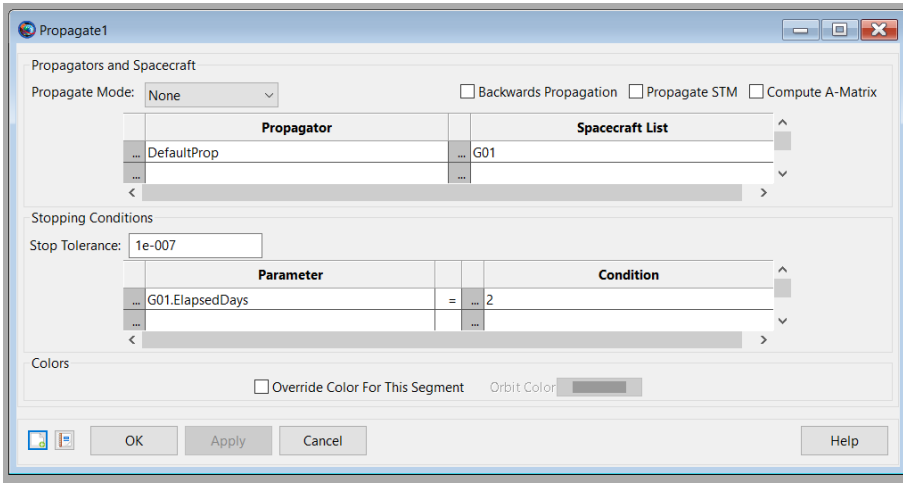

Figure 4-5. Propagate1 Configuration.

4.1.3 Setting up the Event Locator

In this section, the EclipseLocator resource that contains the search criterion will be setup. At the end of a GMAT Simulation, GMAT performs a search on the data it generates and uses that information to go back and calculate the requested information as defined in the event locator part of GMAT. Here, GMAT is setup to specifically generate data concerning the amount of time a satellite spends in the umbral part of an eclipse.

1. Back in the **Resources** Panel, right-click on **Event Locators** and click on **Add → EclipseLocator**.
2. Double-click on the newly-generated **EclipseLocator1**.
3. Under **Spacecraft**, make sure that the satellite defined in Section 4.1.1 is selected.
4. Under **Occulting Bodies**, place a checkmark next to **Earth** and remove any checkmarks that may remain.

5. In the **Eclipse Types** box, remove all the checkmarks except for **Umbra**.
6. Leave all the other remaining settings in their default configuration. The resulting **EclipseLocator** dialog box is shown in Figure 4-6.

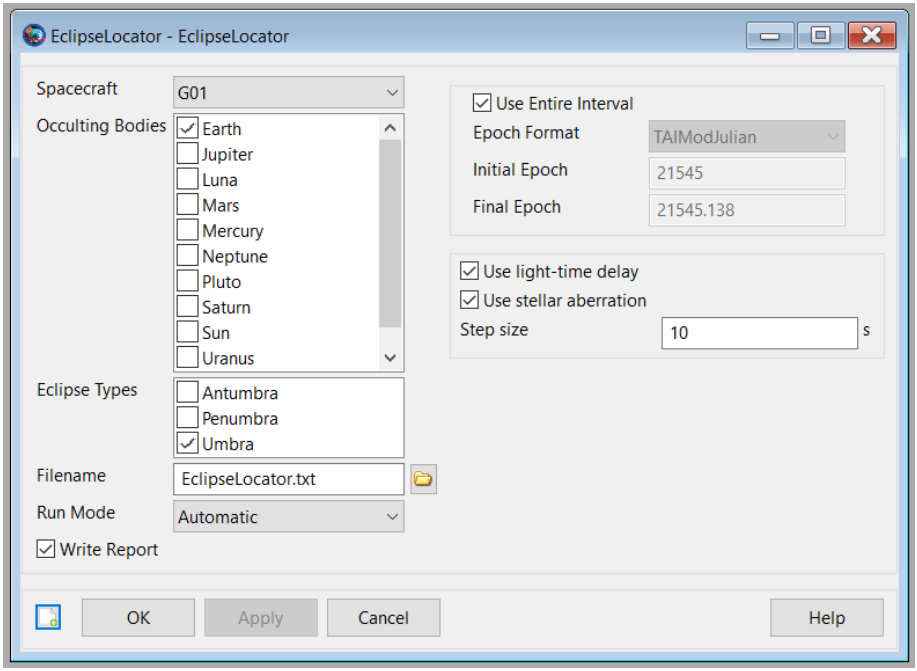

Figure 4-6. Eclipse Locator Configuration.

7. Click on **OK** to close the **EclipseLocator** dialog box and **Save** the document.

4.1.4 GMAT Eclipse Time Results

1. Click on **Run** or press **F5** to run the simulation. GMAT is finished with the simulation when the bottom of the screen shows something similar to Figure 4-7:

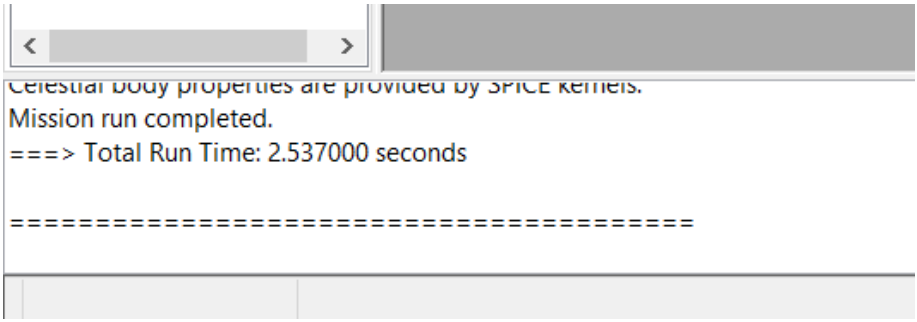

Figure 4-7. GMAT Simulated Mission Complete.

2. Once the simulation is completed, in the **Output** pane, double click on **EclipseLocator** to view the information about the time the satellite spends in the eclipse. The report will look similar to Figure 4-8.

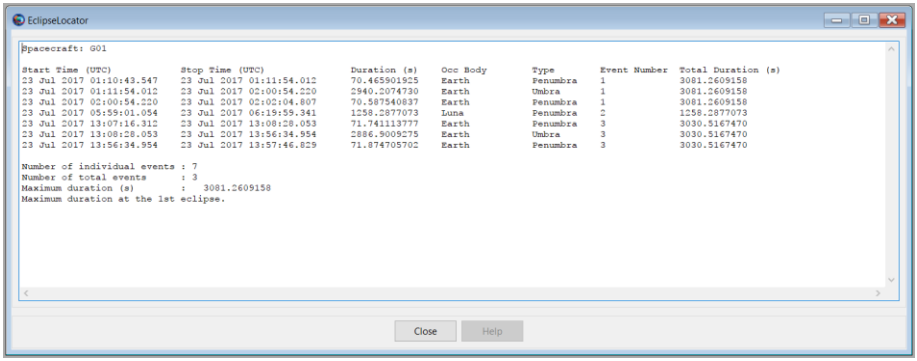

Figure 4-8. GMAT EclipseLocator Report

3. When finished, click on **Close** to close the report. This report is saved on the computer for use outside of GMAT with the filename and location defined in Section 4.1.3.

In Section 4.1.5, the save file from this section is taken and imported into MATLAB where the values assigned to the variables in Section 4.1.1.2 can be modified and the output of GMAT reimported into MATLAB for analysis.

4.1.5 GMAT vs. SGP-4

A tradeoff study was performed between GMAT and the SGP-4 propagator to determine which propagator would be used to develop the results based off of calculated eclipse times. This study was originally based off of

- how computationally expensive a model is,
- in how close the shadow times are to the true value, and
- on which model is representative of a realistic situation.

However, as discussed later in this section, the first bullet point is actually case-sensitive and because of this, it cannot be used as a scoring mechanism in the analysis of the two models.

The computational expensiveness was scored based off of how long the computation took to compute the first full shadow time that the satellite would experience. These results were presented earlier with Table 3-3, Table 3-4, and Table 3-5. Table 4-2 shows a condensed version of these three tables with their individual computation times.

Table 4-2. Computation Time Between the Shadow Models. The values expressed within this table are in seconds.

Model	GRACE	GOCE	CHAMP	Score
ECSM	0.015862	0.013010	0.012736	1
ESCM	0.010652	0.012665	0.024441	2
SGP-4	30.564843	1.260001	12.823254	4
GMAT	4.137995	4.036157	3.958466	3
Real Data	3.553288	3.456365	3.885953	N/A

In Table 4-2, the score column is ranked from the fastest model (1) to the slowest model (4). What is shown is that by using SGP-4 to numerically compute the shadow time, based off of the process presented in

Fundamentals of Astrodynamics and Applications (D. A. Vallado 2007, 303), *Astronomical Algorithms* (Meeus 2009, 171), and *Spacetrack Report #3* (Hoots and Roehrich 1980), *can* be the slowest of the four different models. The fastest model was the ECSM, which was closely followed by the ESCM. However, as shown in Table 4-3, the ECSM produces shadow times that are much further off than the remaining three models.

However, when comparing between SGP-4 and GMAT, for GOCE and CHAMP, it seems like the computation time is case-sensitive and therefore is actually not a good criterion to use for a tradeoff.

Using the same tables presented in Section 3.3.3, the same scoring system can be developed based on how close the shadow times are to the true value. This was scored by taking the average of the percent error for all three satellites. The results are presented in Table 4-3.

Table 4-3. Percent Error in Shadow Times Based off of the True Value. The values presented are expressed as a percent error from the true value except for the Real Data. The Real Data is the true eclipse time expressed in seconds.

Model	GRACE	GOCE	CHAMP	Score
ECSM	25.98%	14.18%	4.36%	4
ESCM	2.23%	0.63%	0.31%	2
SGP-4	0.17%	0.21%	0.03%	1
GMAT	1.59%	1.37%	0.51%	3
Real Data	1520.64	1803.08	2023.64	N/A

From the data presented in Table 4-3, it can be seen that SGP-4 propagator consistently produces errors in the shadow time that are consistently lower than any of the other shadow models. Therefore, by using the SGP-4 propagator, the calculated eclipse times indeed more representative of the derived real-world shadow times.

As what can be seen in Figure 4-9 through Figure 4-14, GMAT does represent a more realistic propagator as comparted to SGP-4. This is because GMAT includes perturbations not present in the SGP-4 model (National Aeronautics and Space Administration 2017) (Hoots and Roehrich 1980). However, since GMAT is not specifically made to im-

port or generate TLEs nor does it have the ability to use any analytical propagator presented in *Spacetrack Report #3* (Hoots and Roehrich 1980), and due to the fact that TLEs are specifically generated and using SGP-4 and using another model would yield inaccurate predictions (Kelso 2014), it was ultimately decided to use the SGP-4 propagator over GMAT for analysis.

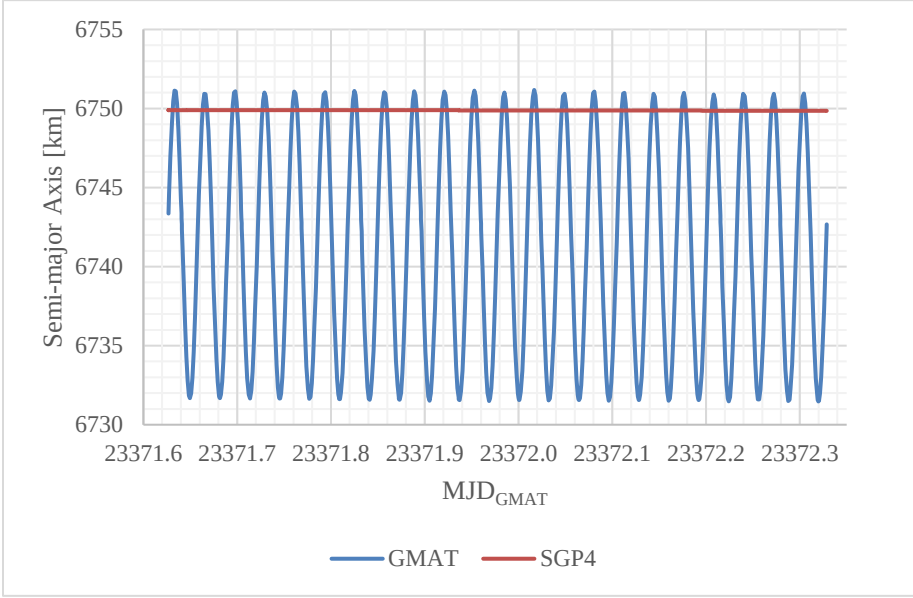

Figure 4-9. Propagated Semi-Major Axis using GMAT vs. SGP-4. This data is representative of the TLE presented in Table 3-4.

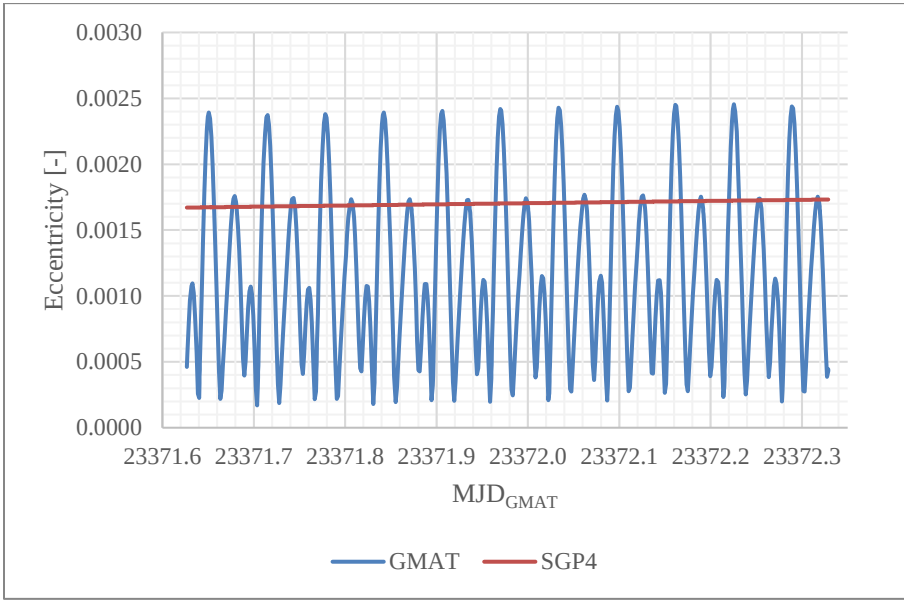

Figure 4-10. Propagated Eccentricity using GMAT vs. SGP-4. This data is representative of the TLE presented in Table 3-4.

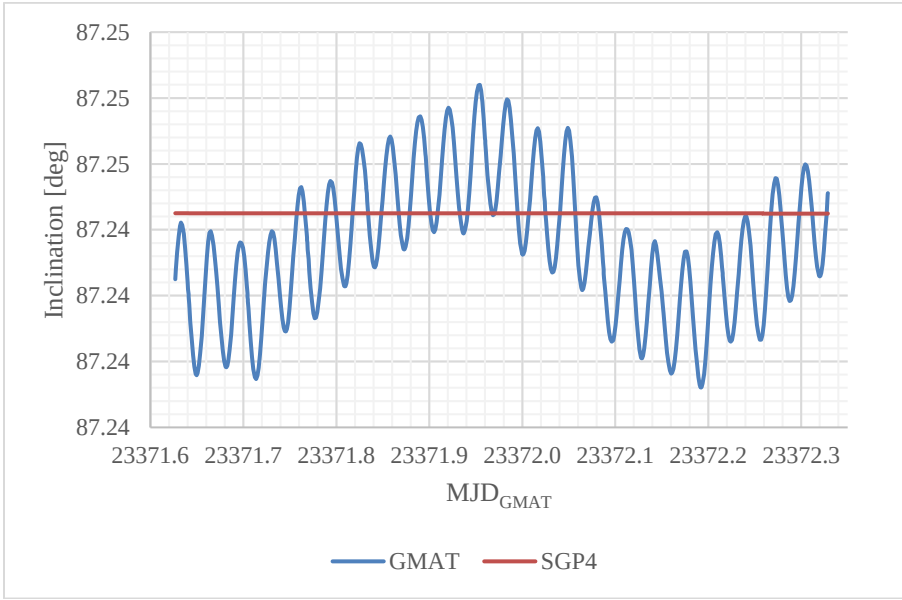

Figure 4-11. Propagated Inclination using GMAT vs. SGP-4. This data is representative of the TLE presented in Table 3-4.

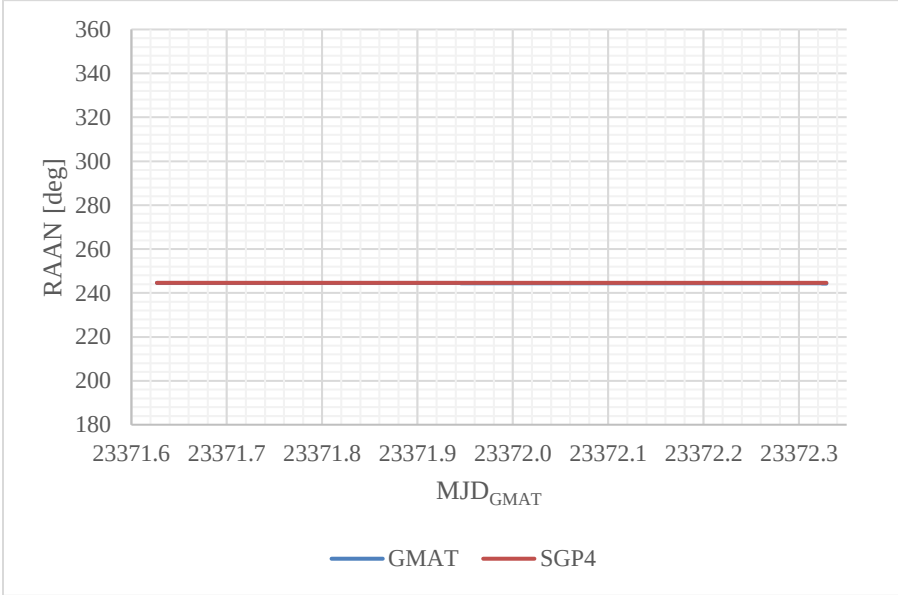

Figure 4-12. Propagated RAAN using GMAT vs. SGP-4. This data is representative of the TLE presented in Table 3-4.

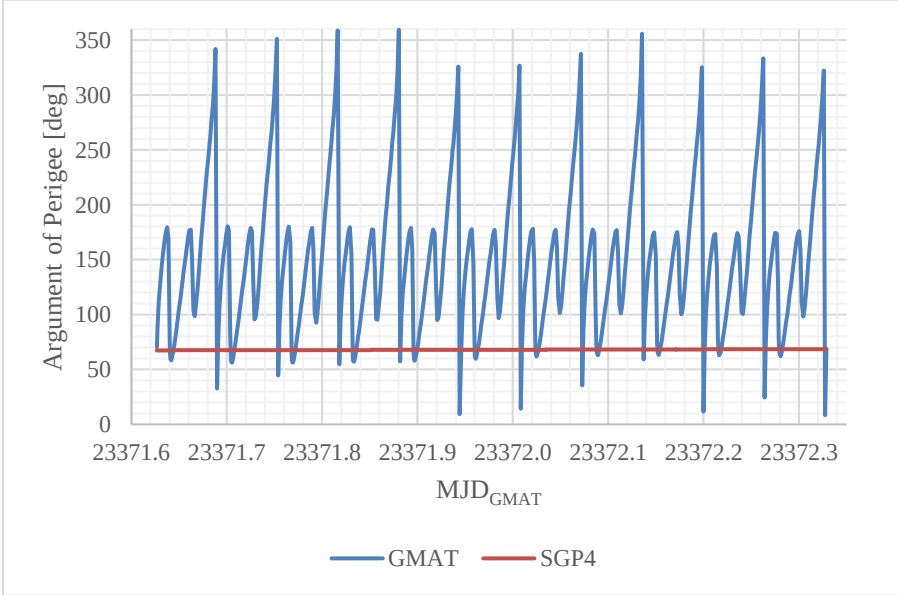

Figure 4-13. Propagated Argument using Perigee of GMAT vs. SGP-4. This data is representative of the TLE presented in Table 3-4.

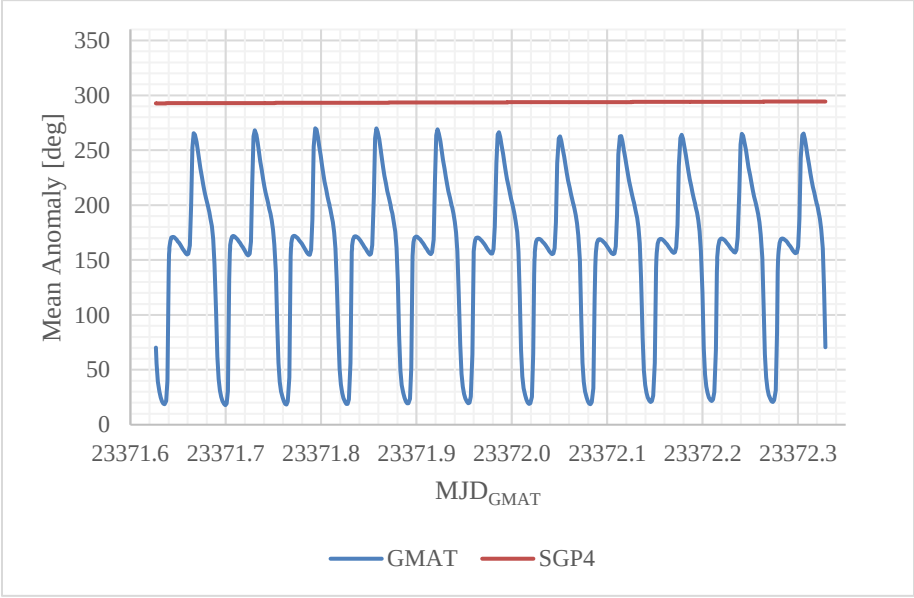

Figure 4-14. Propagated Mean Anomaly using GMAT vs. SGP-4. This data is representative of the TLE presented in Table 3-4.

4.2 MATLAB ANALYSIS SETUP

This section explains how shadow times were analyzed using MATLAB. The overarching methodology was presented earlier in Chapter 1 with Figure 1-2 on page 6. Using this process as a guide, the analysis of the shadow times was structured as a functional program where the minimized difference between *Sigma1* and *Sigma2* can be determined.

First, a general overview of the program is presented from the highest level, showing how the program is structured. Later, the individual blocks will be broken down into a more detailed view where the inputs and outputs of every block are defined as well as an explanation behind the process.

4.2.1 The Top-Level View

The basic structure of the program is as diagramed in Figure 4-15. In the initial setup, the environment variables are cleared and paths are set to allow MATLAB to know the directory path to all subroutines. Once this

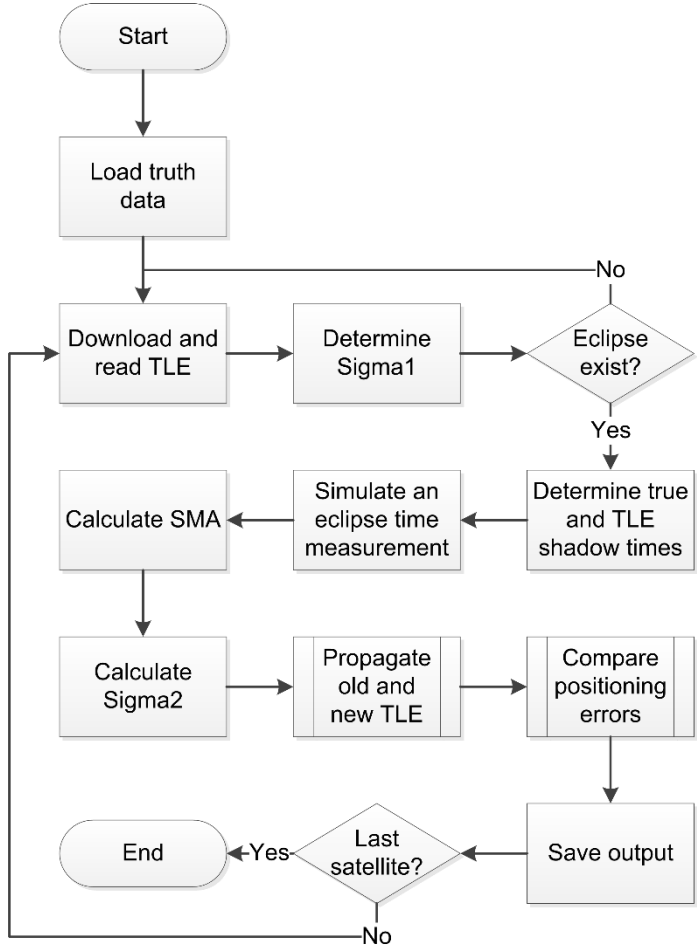

Figure 4-15. Top-Level Flow Diagram.

is completed, truth data text-files are read into the program and are parsed into a structure. The type of data that the program accepts is defined in Section 3.2.1 and marks the entry point of the loop.

Now inside the loop, the program then queries space-track.org to download the TLE for that satellite and parses this information. This happens on every iteration of the loop for every new satellite that is introduced.

Since there is a high probability that the TLE and truth data will not be at the same timestamp, the program propagates the TLE to the near-

est timestamp that exists on the truth data. This allows for the satellite's position to be compared to the position vector of the truth data without a time difference being factored into the analysis.

Next, the truth data is converted to the same reference frame as the SGP-4 propagator, WGS84 ECI, and then into their Keplerian elements. *Sigma1* is then calculated by determining the difference in the semi-major axis between the truth data and the propagated TLE. This value for *Sigma1* is used as the baseline for determining the maximum uncertainty that can exist in measuring the eclipse time of a satellite.

Next, the program determines if an eclipse can theoretically exist. If an eclipse does not exist, the program moves on to the next satellite. If an eclipse is possible, the program uses the process outlined in *Fundamentals of Astrodynamics and Applications* (D. A. Vallado 2007, 303), *Astronomical Algorithms* (Meeus 2009, 171), and *Spacetrack Report #3* (Hoots and Roehrich 1980), or the method presented in Section 3.3.2 to determine the true shadow time and the TLE shadow time. Next the program creates a plethora of uncertainties in the true shadow time "measurement" and converges to a semi-major axis that satisfies that "time measurement." Then, *Sigma2* is calculated by determining the difference in the semi-major axis between the truth data and converged semi-major axis'. The goal here is to find the maximum uncertainty in a measured eclipse time that yields a semi-major axis that is better than the one supplied via a Two-Line Element.

4.2.2 Loading Truth Data

The loading of truth data basically requires one input: the filename. From this, another input is generated and that is the number of lines. With this information, MATLAB reads the data into a structure, sorting everything out as it goes through the file. This process is shown in Figure 4-16.

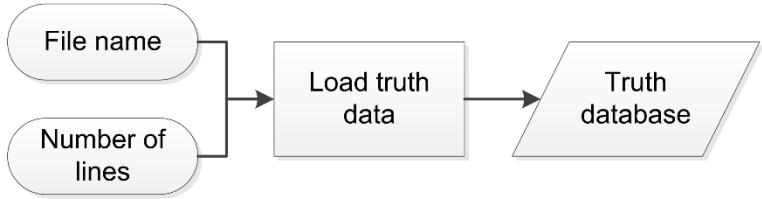

Figure 4-16. Loading Truth Data.

What is of interest for analysis are the positions of the satellites. These are stored under the satellite's name and consists of a structure that contains the three-dimensional position and velocity vector for all *epochs* (converted into Julian Dates as described in Section 3.2.4).

```
PSO =
    epochs: [1×1 struct]
       pos: [77761×3 double]
       vel: [77761×3 double]
     index: 3
```

And for the *epochs* structure:

```
PSO.epochs =
        JD: [77761×1 double]
      year: [77761×1 double]
     month: [77761×1 double]
       day: [77761×1 double]
      hour: [77761×1 double]
    minute: [77761×1 double]
    second: [77761×1 double]
```

This parsed data is then saved as a MATLAB database and remains available for use throughout the program. Anytime this subroutine is called, the program automatically checks to see if the saved-database exists. If it exists, it skips reparsing the data and opens it for use.

4.2.3 Downloading TLEs

Once the truth database has been created, a subroutine is called that downloads all the TLEs that exist for the date range specified in the truth database, also known as *epochs*. The information that is needed to download this data is the start date, end date, NORAD satellite identifier, and the measurement interval.

$$DownloadTLE(SATID, filename, start\ date, end\ date, username, password) \quad (4\text{-}1)$$

The measurement interval is not explicitly given. Therefore, the program was written to dynamically determine this interval. For the supplied data, this interval was ten seconds. This value was used to determine the end date for downloading TLEs.

These inputs are then fed into an MATLAB script API (Equation 4-1) which then fetches the TLEs for the satellite of interest for that particular date range. This data is then saved into a file. This process is shown in Figure 4-17.

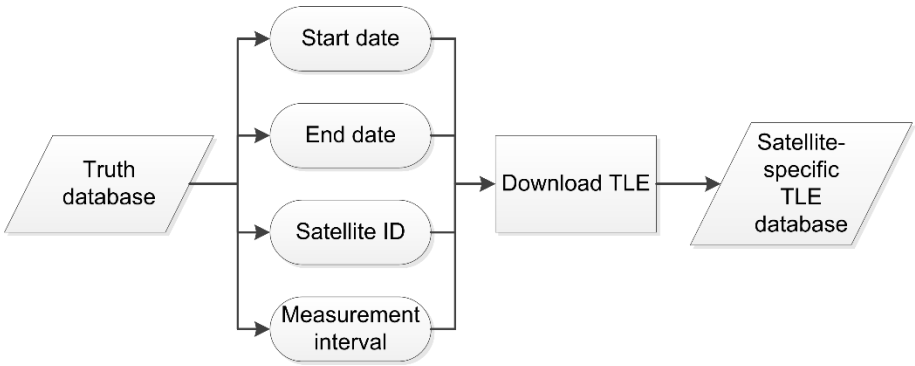

Figure 4-17. Downloading TLEs.

Anytime this subroutine is called, the program automatically checks to see if the TLEs already exist for the specified date range. If they do, the API skips re-downloading the information and just opens it for general use.

4.2.4 Determining *Sigma1*

This next process is a bit more complex and consists of multiple subroutines to get to the error between truth data and the propagated TLE, *Sigma1*. This process is depicted in Figure 4-18. Since the truth data is not in the same coordinate system as the outputted position and velocity vectors from the propagator selected in Section 3.2.2, the truth data is

converted to the same coordinate system as the SGP-4/SDP-4 propagator, ECI, using the process defined in 3.2.6.1.

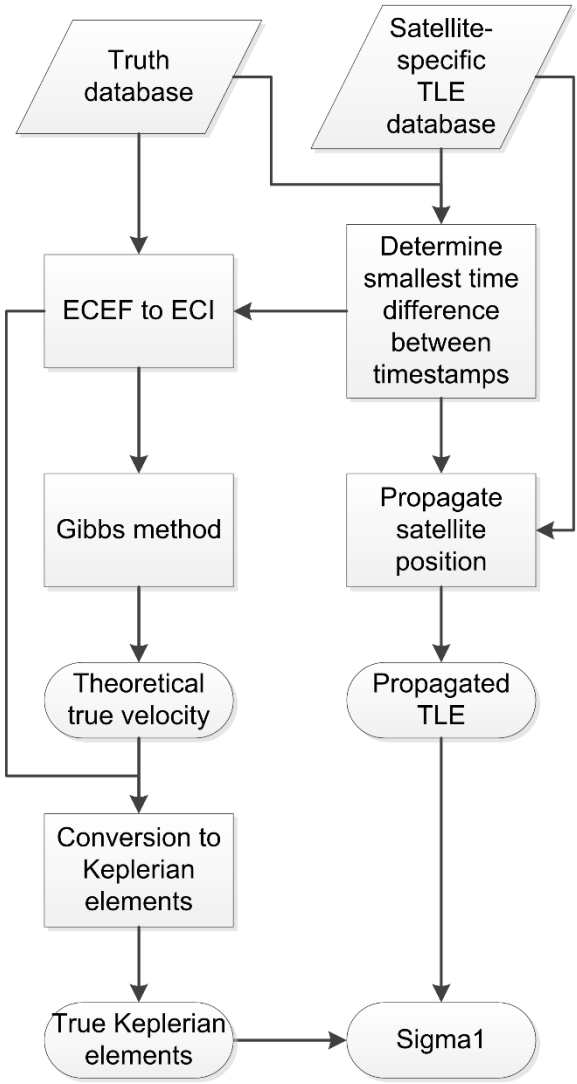

Figure 4-18. Calculating Sigma1.

The first step in determining *Sigma1*, is to propagate the TLE to the nearest forward timestamp that appears on the truth data. In other words, the TLE will always be propagated forward in time up to epoch

interval, expressed in minutes, as defined by the variable *PSO.epochs.JD*. The propagated semi-major axis is then saved for later use in calculating *Sigma1*.

As for the truth database, it is first converted into the ECI coordinate system by means of Section 3.2.6.1. From this, three position vectors are extracted from the database and fed into Gibbs Method, as defined in Section 3.2.7, to calculate the velocity vector, $\boldsymbol{v_2}$, at the timestamp of interest. In Gibbs Method, $\boldsymbol{r_1}$ is the position vector three steps behind the timestamp of interest, $\boldsymbol{r_2}$ is the position vector at the timestamp of interest, and $\boldsymbol{r_3}$ is the position vector three steps forward of the timestamp of interest for LEO satellites. With $\boldsymbol{v_2}$ now calculated, $\boldsymbol{r_2}$ and $\boldsymbol{v_2}$ are converted from the ECI coordinate system into their Keplerian elements. *Sigma1*, the error between truth data and the propagated TLE, is now calculatable via Equation 4-2.

$$Sigma1 = SMA_{TLE} - SMA_{TKE} \tag{4-2}$$

4.2.5 Calculating Shadow Times

Next in the analysis is to determine the shadow time that the TLE says that the satellite will experience, and the *true "measured" shadow time* from what the true positioning data says it will experience. The difference between these two values is the maximum uncertainty used in the sensitivity of the true eclipse time as depicted in Figure 1-2. This process is shown in Figure 4-19.

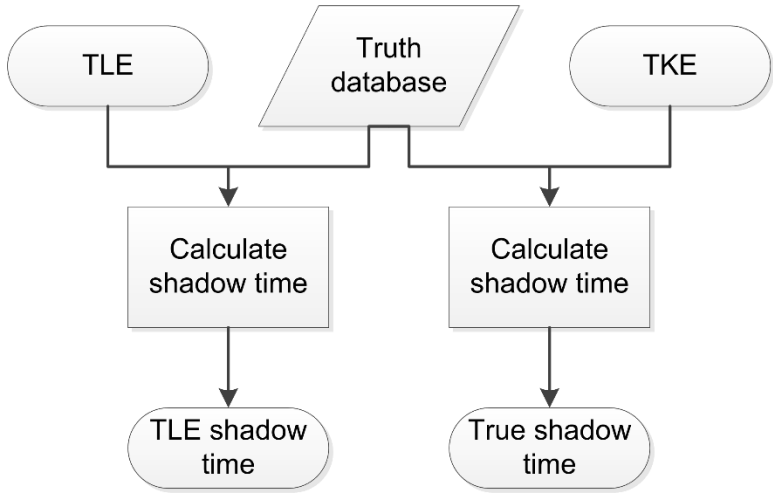

Figure 4-19. Calculating Shadow Times.

Four methods of calculating the eclipse time of the satellite were written. These were the *ECSM*, *ESCM*, SGP-4, and GMAT. However, as previously mentioned in Section 3.3.3, the ECSM model was discarded from analysis due to it diverging from the *ESCM* and GMAT model, and since it had the highest errors when compared to the true semi-major axis (Section 4.1.5).

The method described in Section 3.3.2 was used for a low-resolution first-order approximation of shadow times. For the high-resolution passes, a different technique was utilized that numerically calculates which part of the satellite is for very small timesteps from the epoch that the TLE was generated, logging if it is in the sunlight, penumbra, or umbral part of the eclipse. With all the logged epochs and sun-lit data, the program then calculates the amount of time the satellite spent in the umbral part of the eclipse, according to SGP-4.

For both the high- and low-resolution methods, the same information was passed to the subroutine. And, if a second eclipse does not exist within the specified start- and end- date, the program throws a warning and goes back to downloading the TLE for the next satellite in line for analysis as explained in Section 4.2.3.

4.2.6 Applying Sensitivities to "Measured Data"

This part of the program takes the *true "measured" shadow time* and the TLE shadow time, both as computed in Section 4.2.5, and generates a list of offsets applied to the *true "measured" shadow time* to simulate the shadow time as "measured" aboard the spacecraft with a particular uncertainty in its measurement, i.e. the *offset* in the *true "measured" shadow time*. This process is shown in Figure 4-20.

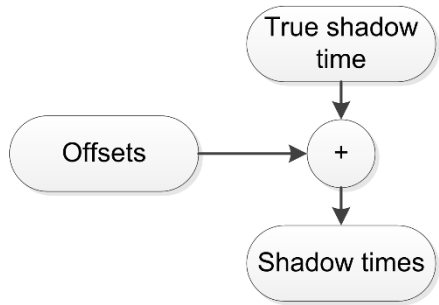

Figure 4-20. Calculating Offsets in Shadow Times.

In short, the *maximum time uncertainty* is calculated as the time difference between the *true "measured" shadow time* and the *TLE shadow time*. This maximum time uncertainty is then linearly spaced from the true "measured" shadow time *minus* the maximum time uncertainty to the true "measured" shadow time *plus* the maximum time uncertainty. Doing so allows for a full sweep of possible "measured" shadow times *below* and *above* the true position of the spacecraft since it is not certain if the satellite's position from the TLE is above or below the true position of the satellites.

4.2.7 Converging upon a Semi-Major Axis

The *measured* shadow time as defined in the previous section is then used in conjunction with the true Keplerian elements to converge to a semi-major axis that satisfies the fed shadow time. This process is shown below in Figure 4-21.

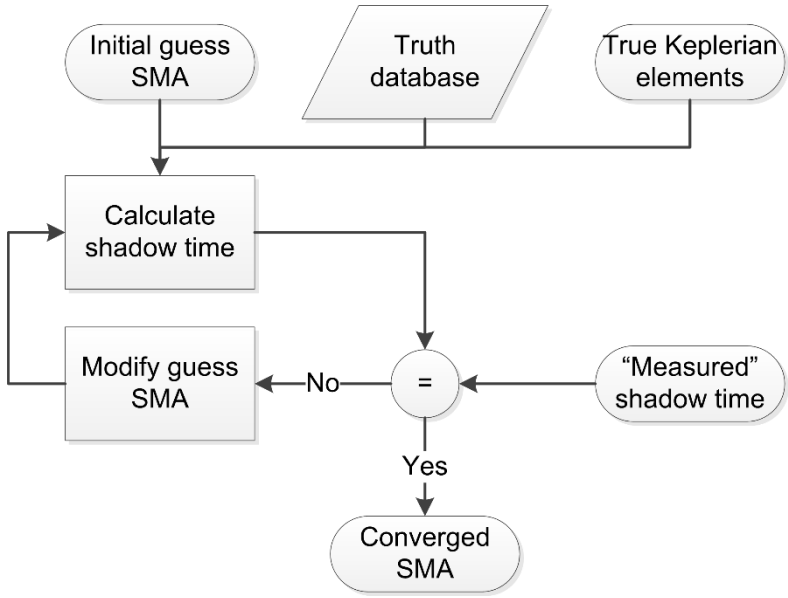

Figure 4-21. Converging to a Semi-Major Axis.

An initial guess in the semi-major axis, the epoch of interest from the truth database, and the true Keplerian elements at that epoch are passed to the subroutine to calculate the shadow time as calculated in Section 4.2.5. The initial guess in the semi-major axis that is used in calculating the shadow time is the semi-major axis of the propagated TLE as calculated in Section 4.2.4. If the calculated shadow time and the offseted shadow time are within the acceptable margin of error, the semi-major axis for the time offset determined in Section 4.2.6 is saved for later analysis. If the calculated shadow time and the "measured" shadow time are above the acceptable margin of error, the initial guess in the semi-major axis is modified such that the loop converges upon a solution.

As for numerical techniques in converging to a solution, a few methods were explored. The most efficient methods were the secant and bisection methods. This was partially due to the number of function evaluations being minimal and in how fast the convergence happens. Since no analytical solution exists for calculating the derivative of shadow times using SGP-4, the derivatives in Newton's and Halley's Method (Appendix G) have to be numerically calculated. If this is coupled with

the SGP-4 routine taking from 1 to 30 seconds per run, it can take a very long time before Newton's Method and Halley's Method to converge to a solution. Table 4-4 shows the number times GMAT would need to open to numerically go through one full iteration. Therefore, the secant method became the method of choice for convergence due to it taking the least amount of function calls per iteration.

Table 4-4. Function Calls per Iteration.

Numerical Convergence Method	Calls per Iteration
Bisection	3
Secant	1
Newton	3
Halley	6

4.2.8 Determining Sigma2

Much like Section 4.2.4, *Sigma2* is calculated in the same manner (Equation 4-3 and 4-4) as *Sigma1*.

$$Sigma2a = SMA_{TKE} - SMA_{calc} \quad 4\text{-}3$$

$$Sigma2b = SMA_{TLE} - SMA_{calc} \quad 4\text{-}4$$

In Figure 4-22, *Sigma2a* is defined as the true minus the converged semi-major axis and *Sigma2b* is defined as the propagated minus the converged semi-major axis.

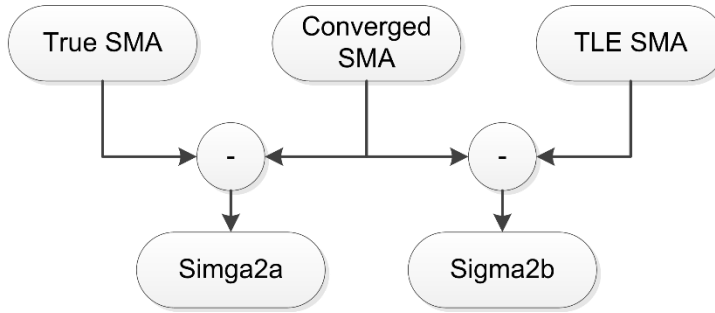

Figure 4-22. Calculating Sigma2.

The calculated quantities for *Sigma2a* and *Sigma2b* are stored for later analysis and these results will be presented in Chapter 5.

4.2.9 Saving the Database

At the end of each run, the following values are stored as an external file and as a structured database: Maximum time uncertainty, offsets, Sigma1, Sigma2a, Sigma2b, and the satellite number (Figure 4-23).

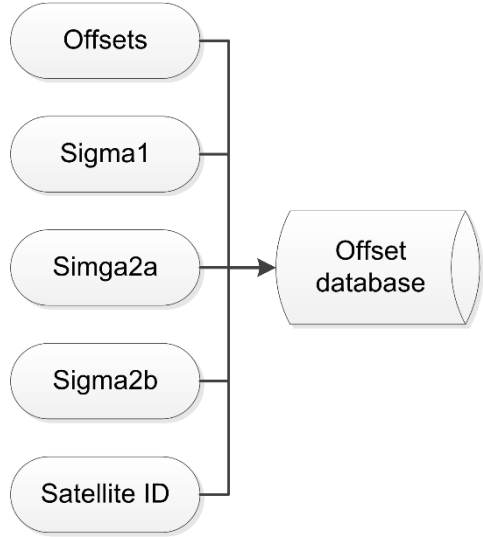

Figure 4-23. Offset Database.

The database is structured as follows for all LEO satellites:

```
offsetDatabase =
    CHAMP:   [1×1 struct]
    GOCE:    [1×1 struct]
    GRACE-A: [1×1 struct]
```

In this database, the only entries that appear are those satellites that have an eclipse between the specified start and end date. Inside each of the satellite identifiers is another structure containing the information found in Figure 4-23 that was calculated throughout Section 4.1.5:

```
offsetDatabase.G29 =
        sigma1: -0.116212222856120
        sigma2: [13×4 double]
```

Going one more level deep, the *sigma2* entry contains the calculated semi-major axis' for the different offsets (Table 5-2).

Lastly, before ending the program, the program checks to see if all the satellites specified in the truth data have been analyzed. If this is not the case, the program moves to the next satellite presented in the truth data and computes its entry for the offset database. Once all satellites from the truth data have been analyzed, the database is saved to a file. This saves on computation times since MATLAB would not need to be run a second time to generate the same results again. The values contained within will be analyzed in Chapter 5.

5 Results, Conclusions, and Recommendations

"The beautiful thing about learning is nobody can take it away from you."

B.B. King

This chapter brings together the theory presented in Chapter 3 and the experimental setup as outlined in Chapter 4 in order to ultimately provide an answer to the research questions presented in Section 1.3. In Section 5.1, these questions are presented once again, but now with their associated answers and results. Section 5.2 presents the main points from Section 5.1. Based upon these results, Section 5.3 lists some recommendations concerning future work on this topic.

5.1 ANSWERING THE RESEARCH QUESTIONS

Within this this section, the research questions and their associated answer are presented.

Question 1:

How can the positioning estimates for small satellites, and inherently low-cost satellites, be improved?

Answer:

In Section 3.2.3, Figure 3-3 through Figure 3-6 show that the associated errors in the orbital elements propagated from one TLE to the next TLE are highest in the semi-major axis. However, since this error is only about 16 meters for small satellites, it represents only a 0.02% difference when studying satellites at an altitude of 400 kilometers. Nevertheless, to determine where this large change comes from, the errors associated with the cross-track, along-track, and radial position need to be examined.

With respect to the cross-track, along-track, and radial sources of errors presented in Section 2.1, the cross-track velocity component is usually the smallest (Vallado and Agapov 2010, 7). The cross-track velocity error sources mainly stem from the inclination and the right ascension of the ascending node. By consulting Figure 3-5 and Figure 3-6, the errors between two successive TLEs for a years-worth of TLEs are indeed small. Therefore, the errors found in Figure 3-2 would either have to stem from the along-track or radial direction of the satellite. However, according to Table 1-1, the uncertainty in the radial direction is much smaller than the along-track and cross-track components, so the error in the radial direction can be considered to be minimal in Figure 3-2.

Therefore, the along-track error seems to contribute the most to the positioning error of the satellite. This error can be contributed to two main factors: *drag* and *time synchronization*. Drag forces primarily dominate orbits below 800 kilometers (Wertz, et al. 1997, 270). On the other hand, no matter the altitude of the satellite, time synchronization plays just as important of a role in positioning errors due to velocities being highest in this direction. Therefore, still having an accurate on-board system clock in conjunction with measurement data at a high refresh rate

can prove to be useful in providing high-resolution data to ground station controllers in keeping up with the everyday operations of the spacecraft and in improving upon orbital elements.

What can be concluded is that due to drag forces, a satellite in LEO experiences the largest change in its along track-position. However, by examining the Keplerian elements of a satellite, Figure 3-3 shows that the largest change in TLE Keplerian elements is in the semi-major axis. Therefore, improvements can be made in the positioning estimates of a spacecraft by measuring some physical quantity the satellite experiences to a high degree of accuracy in time resolution where the semi-major axis plays an important factor.

Question 2:

Is there some piece of orbital information that can be used to improve upon positioning estimates?

Answer:

One physical quantity that satellites experience that would require time synchronization *and* the semi-major axis is the amount of time it spends eclipsed by Earth. This thesis explored the possibility of measuring this eclipse time and to what uncertainty it must be measured to provide sufficient data to make improvements. How this eclipse time is measured could be different for every satellite, whether it be measured by a dedicated instrument or by data derived from other instruments. What this instrument might be, is beyond the scope of this report. The driving requirement of this theoretical instrument and to what accuracy is explained in the answer to question four.

Question 3:

What parameters are influenced by this information?

Answer:

By differentiating Equation 3-49 and assuming k, the percentage of time where the satellite is eclipsed, to remain constant for small changes in the semi-major axis, a, the derivative can be taken of the equation for

the shadow time (Equation 5-1) with respect to the semi-major axis. Equation 5-2 results.

$$\frac{\partial}{\partial a} T_{SH} = \frac{\partial}{\partial a}\left(k \cdot 2\pi \sqrt{\frac{a^3}{\mu}} \right) \quad 5\text{-}1$$

$$\frac{\partial T_{SH}}{\partial a} \cong 3\pi k \sqrt{\frac{a}{\mu}} \quad 5\text{-}2$$

What this equation shows is that for satellites farther away from Earth, the change in the amount of time a satellite is eclipsed by Earth will be more than that at lower altitudes. Therefore, the farther away a satellite is from Earth, the more sensitive the shadow time becomes. In Equation 5-2, k is influenced by the inclination, semi-major axis, and right ascension of the ascending node of the satellite, the equatorial coordinates of the Sun, and the instantaneous distance to the Sun (Equations 3-48 through 3-52); however, since the equatorial coordinates and distance to the sun remain stable, the parameters that most influence k are the inclination, semi-major axis, and right ascension of the ascending node of the satellite. Taking this one step further, as with what can be seen in Figure 5-1, the inclination and right ascension of the ascending node oscillate with a much smaller amplitude than the semi-major axis.

Therefore, the main parameter that influences the percentage of time a satellite spends in eclipse is the semi-major axis. Figure 5-2 shows how the shadow time, orbital period, and the percentage of the orbit in eclipse vary as a function of the altitude.

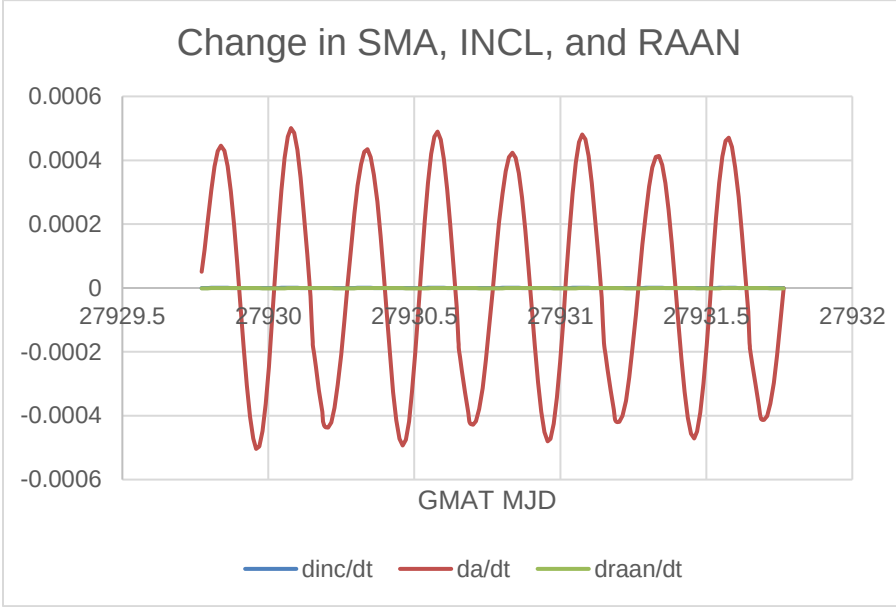

Figure 5-1. The Slow Variables that Influence the Variable, *k*.

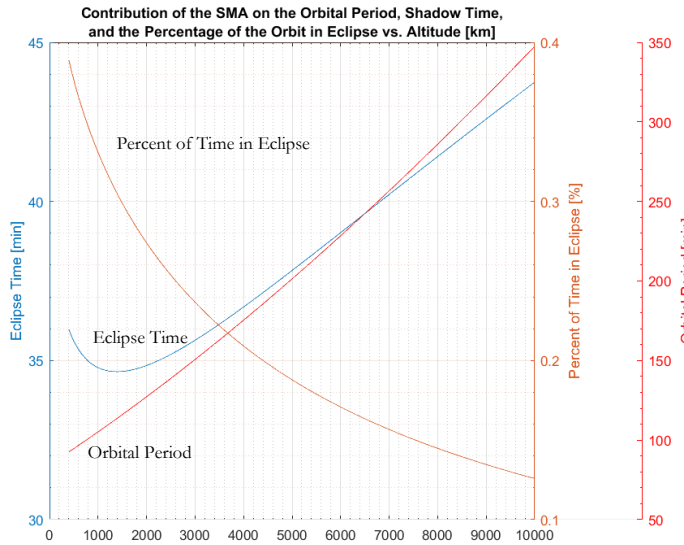

Figure 5-2. Contribution of the Semi-Major Axis on the Orbital Period, Shadow Time, and the Percentage of the Orbit in Eclipse. This figure was computed for a phase angle of zero degrees using the method described in Section 3.3.2.

By using the ECSM model under the same assumptions and conclusion as outlined in Section 3.3, where k is no longer constant, Equation 5-3 and 5-4 result.

$$\frac{\partial T_{SH}}{\partial a} = \frac{3\sqrt{a}\cos^{-1}\left(\sec\beta\sqrt{1-\left(\frac{R_E}{a}\right)^2}\right)}{\sqrt{\mu}} - \frac{2R_E^2\sec\beta}{\sqrt{\mu}\,a^{\frac{3}{2}}\sqrt{1-\left(\frac{R_E}{a}\right)^2}\sqrt{1-\sec^2\beta\left(1-\left(\frac{R_E}{a}\right)^2\right)}} \tag{5-3}$$

$$\frac{\partial T_{SH}}{\partial \beta} = \frac{2a^{\frac{3}{2}}}{\sqrt{\mu}} \cdot \frac{-\tan\beta\sec\beta\sqrt{1-\left(\frac{R}{a}\right)^2}}{\sqrt{1-\left(1-\left(\frac{R_E}{a}\right)^2\right)\sec^2\beta}} \tag{5-4}$$

What is shown is that by differentiating the ECSM model, it is hard to see any useful information about how a certain variable influences the shadow time from an analytical expression. Thus, a numerical approach was more appropriate for analysis. However, what can be seen is that the

$$\frac{3\sqrt{a}}{\sqrt{\mu}} \tag{5-5}$$

term from Equation 5-2 is also apparent in the first part of Equation 5-3. Therefore, the first part of Equation 5-3 concerns the change in the period and the second part of the equation concerns the change in the percentage of time a satellite is eclipsed. And as previously stated, the main contributing factor to these derivatives just happens to also be the semi-major axis.

Question 4:
What are the requirements of such an instrument?

Answer:
In Table 5-1, the calculated semi-major axis does improve for *two* out of the *three* satellites analyzed in LEO assuming no uncertainty in measuring the eclipse time. The reasoning behind why one satellite does not seem to produce a better semi-major axis, needs to be further investigated to develop a definitive answer. However, what this table suggests is that for very-low-altitude satellites, where drag forces are higher, this method *can* calculate a semi-major axis that seems to be worse. Nevertheless, what can be seen is that for satellites flying at higher altitudes, the calculated semi-major axis leans more towards the true value than the TLE's.

Table 5-1. Comparison of Semi-Major Axes. All units are expressed in kilometers and assuming no uncertainty in measurements.

Model	GOCE	CHAMP	GRACE-A
TLE	6605.47	6743.35	6850.01
Calculated	6603.03	6738.68	6847.75
True	6611.29	6740.17	6846.95

Table 5-2 shows the calculated semi-major axes as a function of uncertainties in the eclipse time measurements. The maximum allowed uncertainty in an eclipse time measurement is the location where the calculated semi-major axis is the same as that found in a TLE. This value is about 2.56 seconds (0.169% of the true shadow time) for GRACE-A and about 0.6 seconds (0.033% of the true shadow time) for CHAMP.

Table 5-2. Comparison of Calculated Semi-Major Axes with Uncertainties in the Measured Eclipse Time. All units are expressed in kilometers.

Eclipse Time Uncertainties [s]	Calculated Semi-Major Axes [km]	
	CHAMP	GRACE-A
-10.0	-	6856.45
-5.0	-	6852.19
- 1.0	6740.60	6848.68
- 0.8	6740.22	6848.46
- 0.6	6739.83	6848.33
- 0.4	6739.44	6848.11
- 0.2	3739.06	6847.93
0.0	6738.68	6847.75
+0.2	6738.29	6847.58
+0.4	6737.91	6847.40
+0.6	6737.53	6847.30
+0.8	6737.14	6847.13
+1.0	6736.76	6846.95
+5.0	-	6843.51
+10.0	-	6839.20
TLE	6743.35	6850.01
True	6740.17	6846.95

However, that is only half the problem as the standard deviation in the calculated semi-major axis also needs to be taken into account. The results are shown in Table 5-3.

Table 5-3. Standard Deviation in Eclipse Time Uncertainties. The variance for the various uncertainties was calculated by taking the calculated semi-major axis for both the positive and negative uncertainty value.

Eclipse Time Uncertainties [s]	Standard Deviation in the Calculated Semi-Major Axis [km]	
	CHAMP	**GRACE-A**
0.0	0.00	0.00
0.2	0.38	0.18
0.4	0.77	0.36
0.6	1.15	0.51
0.8	1.54	0.66
1.0	1.92	0.87
5.0	-	4.34
10.0	-	8.62
SMA_{TLE}-SMA_{TKE}	3.18	3.06

Therefore, by using this 2.56-second uncertainty for CHAMP, the calculated semi-major axis would have an uncertainty of about 2.2 kilometers. This would be unacceptable since Figure 3-3 definitely shows that the semi-major axis changes by a much smaller amount between successive TLEs.

To account for this, a curve was fitted across the data presented in Table 5-3 to determine the location where the standard deviation is equal to average change in the semi-major axis between successive TLEs (Figure 3-3). Using this table and figure allows for the theoretical maximum uncertainty in measuring eclipse times to be calculated for satellites based upon their size. Thus, such a device capable of measuring the eclipse interval for a small satellite in LEO would need to be able to measure the eclipse interval to an uncertainty of about 0.01 seconds or better (about 0.02% of the orbital period). This eclipse time uncertainty not only assures for a low standard deviation in the calculated semi-major axis, but also in providing a calculated semi-major axis that is consistently closer to the true semi-major axis.

With this said, it should be noted that more LEO satellites should be studied to further refine this number. Nevertheless, what this method shows is that a semi-major axis can be calculated from measuring eclipse times and to what uncertainty this measurement needs to be determined.

Question 5:

Can the positioning error of the satellite be improved with this additional information?

Answer:

Unfortunately, even though the calculated semi-major axis is closer to the true semi-major axis than what is supplied on a TLE, the absolute positioning error is initially worse and grows over time (Figure 5-3 and Figure 5-4). This larger positioning error can be explained due to the fact that TLEs already represent the best possible solution given the data points used to generate them and any deviation from these numbers will result in errors with a magnitude that is heavily dependent on the type of orbit (Kelso 2014). These figures show the development of the positioning error for CHAMP. Figures related to the development of the individual orbital elements, positioning errors, and the location with respect to the true, TLE, and modified TLE position are found in Appendix E and Appendix F.

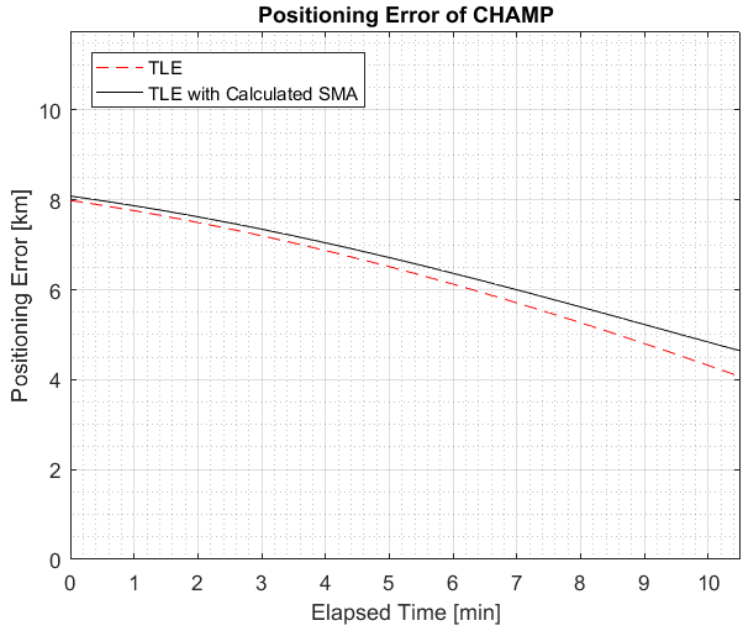

Figure 5-3. Relative Positioning Error of CHAMP for the First 10 Minutes.

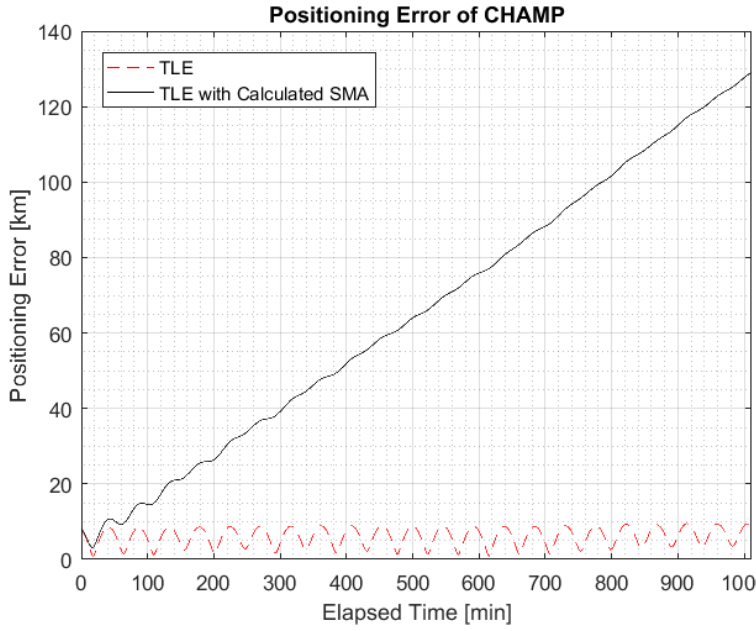

Figure 5-4. Relative Positioning Error of CHAMP with Respect to the True Position.

5.2 CONCLUSION

The largest error in the Keplerian elements is in the along-track direction. This error can be contributed to two main factors: *drag* and *time synchronization*. Drag forces primarily dominate orbits below 800 kilometers. Time synchronization is just as important in positioning errors due to velocities being highest in this direction.

Next, the error of successive propagated TLEs were examined to determine that the largest contributing factor to the position error was from the semi-major axis. This thesis then focused on developing a driving system requirement that uses time synchronization and eclipse intervals to calculate a semi-major axis.

This semi-major axis was then analyzed for multiple eclipse time uncertainties to calculate the standard deviations of the calculated semi-major axes. With this information, it was found that such a device would need to be capable of measuring eclipse intervals to an uncertainty not to exceed 0.01 seconds (about 0.02% of the orbital period).

Though this calculated semi-major axis was indeed closer to the real value, the positioning estimates were further away. Because of this, the calculated semi-major axis must not be used in place of the one derived from the TLE. In doing so, a divergence from the "best fit" data is observed. Nevertheless, this thesis shows that it is possible to calculate a semi-major axis from eclipse times and to what uncertainty this measurement must be determined.

5.3 RECOMMENDATIONS FOR FUTURE WORK

The following are recommendations for future work to be performed on this topic to improve upon the results presented in Section 5.1. The recommendations in this section are categorized by chapter and given as an unordered list.

Theoretical Approach:

- There seems to be a lack of POD data available to the general public when it comes to LEO Satellites. Find this LEO POD information.

- Other orbit propagators aside from those listed in Spacetrack Report #3 exist. It might be worth investigating the parent non-simplified theory of the SGP-4/SDP-4 theory in order to further tweak the results (IGP-4 and AFGP-4).
- In converting between the ECEF and the ECI reference frame, just using the GMST transformation matrix is often exercised and seldom documented. This report documented *and* used the full transformation matrix. However, Equations 3-8 through 3-10, and 3-13 are very much empirical formulas that have not been updated since the 1970s. The terms in these formulas could possibly be updated to provide even better results.
- Perform the same analysis using differential correction across all of the orbital elements.

Experimental Setup:

- Investigate the use of AGI's STK as an alternative to NASA's GMAT, which includes the SGP4 propagator.
- In converging upon a semi-major axis, the *fzero()* subroutine supplied by MathWorks does not necessarily converge to a solution all the time. This can be a problem when setting the analysis up to run automatically. Fortunately, other methods, like the Secant Method, work. Investigate the use of other numerical techniques to converge to a solution faster.
- With respect to the database that is mentioned in Section 4.2.9, it contains a table of offsets and errors. This table was used to write an equation to solve for an offset for a user-supplied error. Instead of solving for an offset this way, improvements can be made by solving for the required measured eclipse time instead.

General Recommendations:

- Investigate the reason why using three position vectors from a POD file to generate the velocity vector give better results vs. using the supplied velocity vector from the POD, even after

accounting for the rotation of Earth. Furthermore, how much different would the results be if a method other than Gibbs Method was used?

- Perform the same analysis with more LEO satellites with POD information to better converge upon an uncertainty. Perform this analysis for satellites with different RADAR cross-sectional areas.
- There doesn't seem to be any quick method available to convert between ITRF14 and WGS84 in the sub-10-centimeter level. Converting at this level, some uncertainty is gained. Develop a method to convert between these two reference frames while keeping the same resolution.

Appendix A. LIST OF VARIABLES

$ABCD$	Rotation Matrix between ECEF and ECI
AU	Astronomical Unit
D	Gregorian Calendar Day + Fractional Part of the Day
JD	Julian Day/Date
M	Mean Anomaly
	Gregorian Calendar Month
P	Orbital Period of a Satellite
$\boldsymbol{R}$	Satellite Position Vector
$R_\oplus$ or R_E	Mean Radius of the Earth
R_S	Mean Radius of the Sun
R_x	Rotation Matrix about the x-axis
R_y	Rotation Matrix about the y-axis
R_z	Rotation Matrix about the z-axis
T	Julian Century
T_{SH}	Eclipse Time
$\boldsymbol{V}$	Satellite Velocity Vector
Y	Gregorian Calendar Year

a	Semi-Major Axis
e	Eccentricity
h	Angular Momentum Vector
i	Inclination
$i_\odot$	Phase Angle
n	Node Vector
r	Satellite Position Vector
v	Satellite Velocity Vector
x_p	Angular Displacement Along the Zero Meridian
y_p	Angular Displacement Normal to the Zero Meridian

$\measuredangle H$	The Apparent minus The Mean Sidereal Time
$\measuredangle t$	The Difference Between UTC and UT1
$\measuredangle \varepsilon$	Nutation in the Obliquity of the Ecliptic
$\measuredangle \psi$	Nutation in the Longitude

Λ	A Function of GMST at 0h UT1
Ω	Right Ascension of the Ascending Node
$\bar{\epsilon}$	Mean Obliquity of the Ecliptic
μ	Gravitational Parameter
a	Right Ascension
δ	Declination
ϵ	True Obliquity of the Ecliptic
θ_0	GMST
ρ_c	Shadow Cone Convergence Angle
τ	Eclipse Time
υ	True Anomaly
ψ	Nutation in Longitude
ω	Argument of Perigee
ω^*	Earth's Rotation Rate in a Precessing Frame

Appendix B. List of Acronyms

AFGP	Air Force General Perturbation
AOP	Argument of Perigee
API	Application Program Interface
CFR	Code of Federal Regulations
DLR	Deutsches Zentrum für Luft- und Raumfahrt
DP-4	Deep-Space Perturbation Theory #4
ECC	Eccentricity
ECEF	Earth-Centered, Earth-Fixed
ECI	Earth-Centered Inertial
ECSM	Earth Cylindrical Shadow Model
EOP	Earth Orientation Data
ESCM	Earth Shadow Conical Model
GMAT	General Mission Analysis Tool
GMST	Greenwich Mean Sidereal Time
GPS	Global Positioning System
IGP	Unknown
INC	Inclination
ISS	International Space Station
ITAR	International Traffic in Arms Regulations
ITRF	International Terrestrial Reference Frame
LEO	Low Earth Orbit
MATLAB	Matrix Laboratory
MA	Mean Anomaly
MEO	Medium Earth Orbit
NASA	National Aeronautics and Space Administration
NGIA	National Geospatial-Intelligence Agency
NOAA	National Oceanic and Atmospheric Administration
NORAD	North American Aerospace Defense Command
RAAN	Right Ascension of the Ascending Node
RADAR	Radio Detection and Ranging
RMS	Root Mean Square
SCC	Space Computation Center
SDP	Simplified Deep-Space Perturbation

SDP4	Simplified Deep-Space Perturbation Theory #4
SDP8	Simplified Deep-Space Perturbation Theory #8
SGP	Simplified General Perturbation
SGP4	Simplified General Perturbation Theory #4
SGP8	Simplified General Perturbation Theory #8
SMA	Semi-Major Axis
SRP	Solar Radiation Pressure
TA	True Anomaly
TKE	True Keplerian Element
TLE	Two-Line Element
UT	Universal Time
UT0	"Raw" Uncorrected UT
UT1	UT0 Corrected for Polar Motion
UTC	Coordinated Universal Time
WGS	World Geodetic System

Appendix C. TLE EXAMPLE

The following TLE was generated for the International Space Station on 8 October 2016 at 01:05:00 UTC. The first line is not a part of a TLE and only appears here to serve as a guide in counting column numbers.

```
123456789 123456789 123456789 123456789 123456789 123456789 123456789
1 25544U 98067A   16280.54513569  .00016717  00000-0  10270-3 0  9035
2 25544  51.6411 222.5831 0007033  41.1186 319.0496 15.54057571 22306
```

Column	Content	Example
LINE 1		
1	TLE Line Number	1
7-Mar	Satellite Number	25544
8	Satellite Classification	U - Unclassified
17-Oct	International Designator	98067A
19-32	Epoch Time	16280.55
34-43	$\dot{n}_0/2$	0.000167
45-52	$\dot{n}_0/6$	00000-0
54-61	B*	1.03E-04
63	Ephemeris Type (Unused)	0
65-68	Element Set Number	903
69	Modulus 10 Checksum	5
LINE 2		
1	TLE Line Number	2
7-Mar	Satellite Number	25544
16-Sep	Inclination	51.6411 [deg]
18-25	RAAN	222.5831 [deg]
27-33	Eccentricity	0.0007033 [-]
35-42	Argument of Perigee	41.1186 [deg]
44-51	Mean Anomaly	319.0496 [deg]
53-63	Mean Motion	15.54057571 [Orbits/day]
64-68	Number of Orbits	2230
69	Modulus 10 Checksum	6

Appendix D. TLEs Used in this Report

GOCE

```
1 34602U 09013A   13203.15484632  .00001568  19245-5  14308-5 0  9997
2 34602 096.5624 231.9792 0007079 019.3980 054.9006 16.17136440254889
```

CHAMP

```
1 26405U 00039B   05001.12673604  .00010487  00000-0  95200-4 0  9994
2 26405 087.2425 244.6120 0004627 070.5496 289.6343 15.67794191253225
```

GRACE-A

```
1 27391U 02012A   05001.17201054  .00002419  00000-0  78765-4 0  9996
2 27391 089.0240 219.2330 0015153 311.7148 048.2843 15.31318717155891
```

Appendix E. PROPAGATED TLE FOR CHAMP

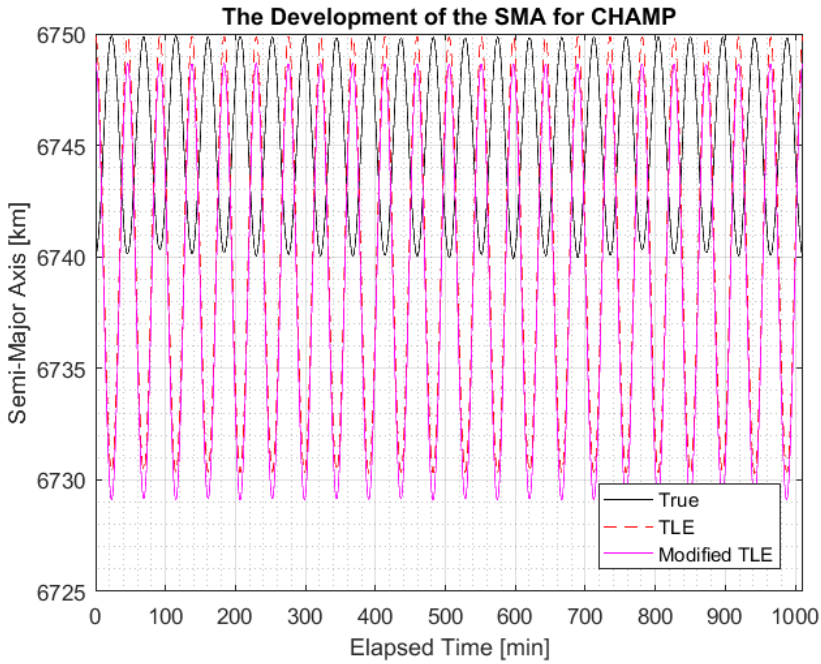

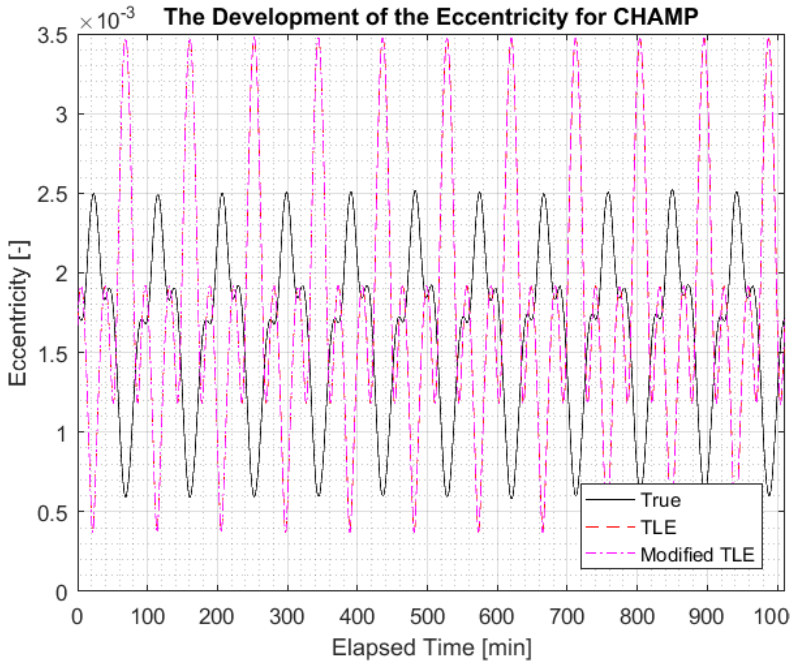
The Development of the Eccentricity for CHAMP
×10^-3
Eccentricity [-]
Elapsed Time [min]
True
TLE
Modified TLE

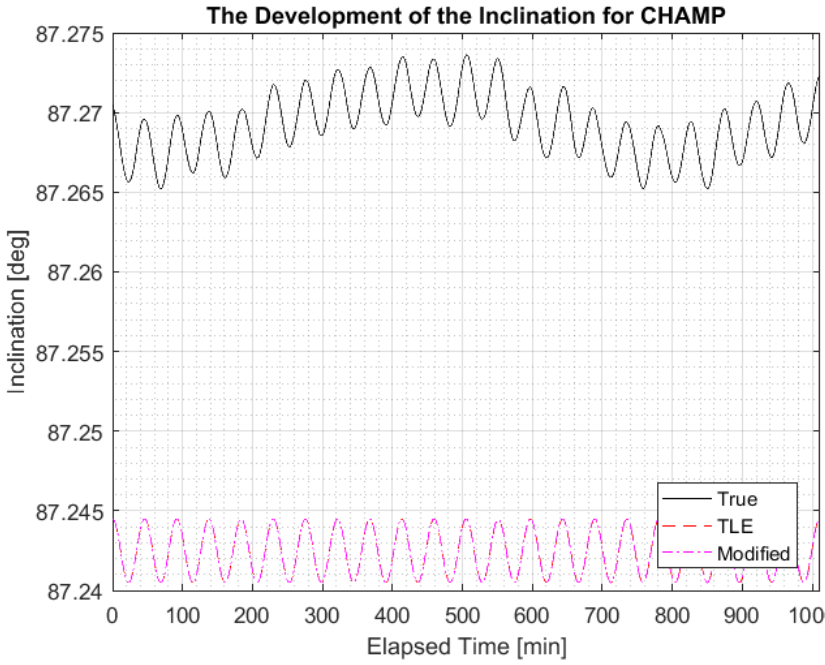
The Development of the Inclination for CHAMP
Inclination [deg]
Elapsed Time [min]
True
TLE
Modified

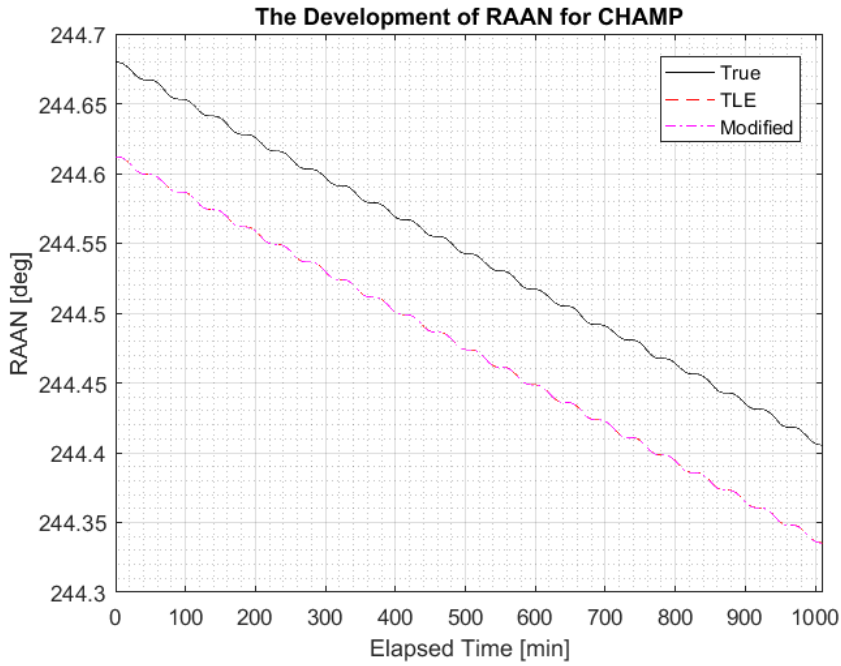
The Development of RAAN for CHAMP
RAAN [deg]
Elapsed Time [min]
True
TLE
Modified
244.7
244.65
244.6
244.55
244.5
244.45
244.4
244.35
244.3
0
100
200
300
400
500
600
700
800
900
1000

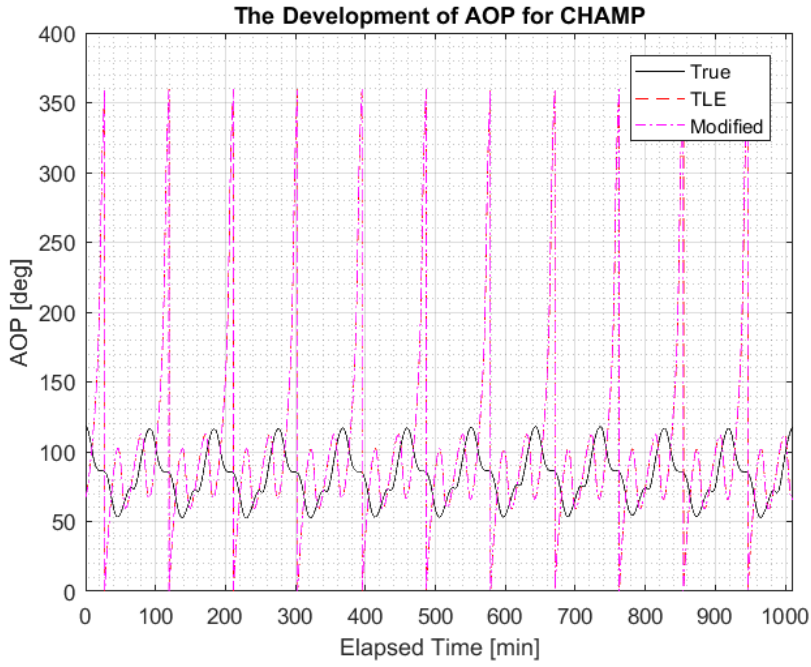
The Development of AOP for CHAMP
AOP [deg]
Elapsed Time [min]
True
TLE
Modified
400
350
300
250
200
150
100
50
0
0
100
200
300
400
500
600
700
800
900
1000

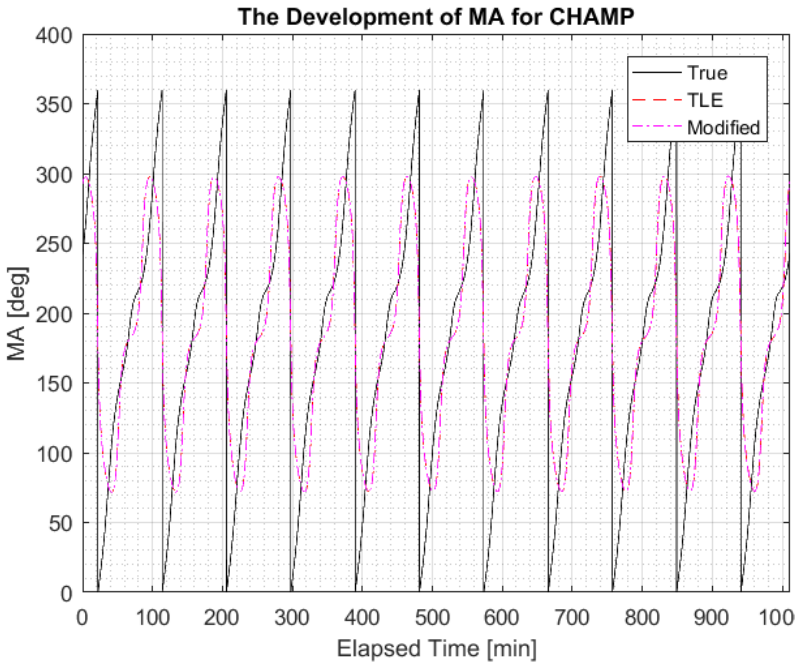
The Development of MA for CHAMP
True
TLE
Modified
MA [deg]
Elapsed Time [min]
0
50
100
150
200
250
300
350
400
0
100
200
300
400
500
600
700
800
900
1000

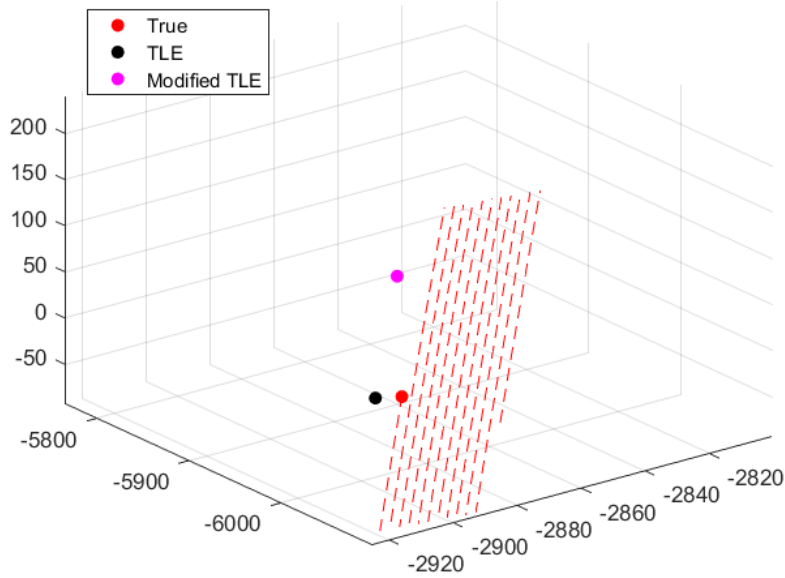
True
TLE
Modified TLE
200
150
100
50
0
-50
-5800
-5900
-6000
-2920
-2900
-2880
-2860
-2840
-2820

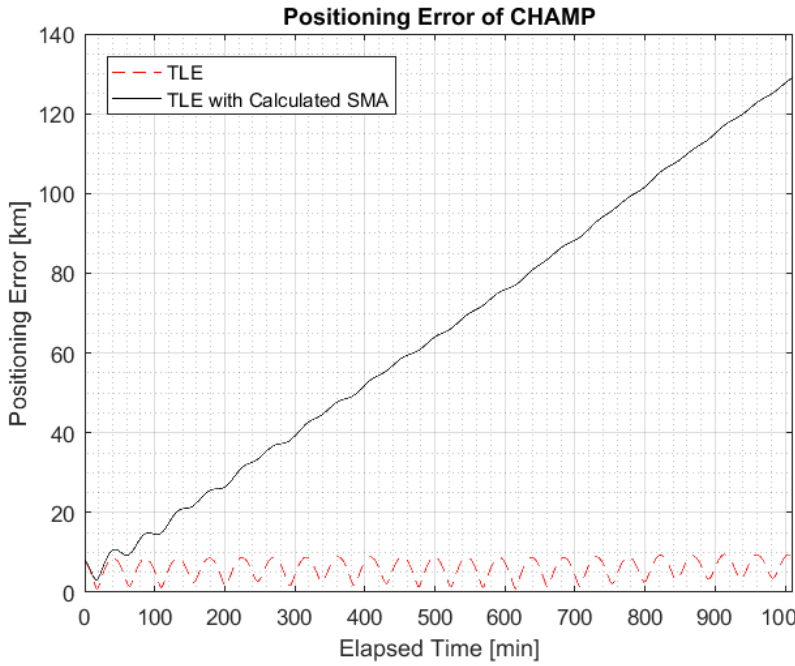
Positioning Error of CHAMP
TLE
TLE with Calculated SMA
Positioning Error [km]
Elapsed Time [min]
0
20
40
60
80
100
120
140
0
100
200
300
400
500
600
700
800
900
1000

Appendix F. PROPAGATED TLE FOR GRACE-A

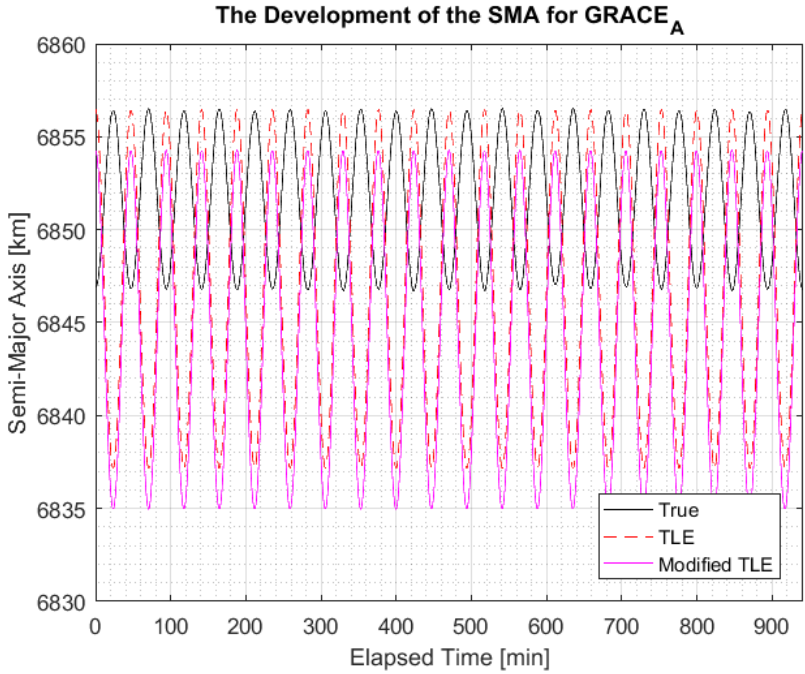

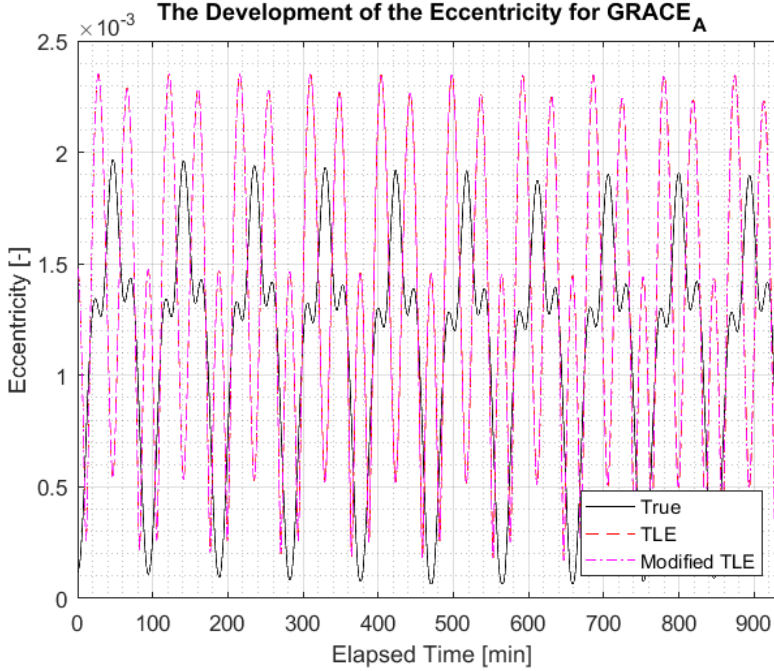
The Development of the Eccentricity for GRACE A
×10^-3
2.5
2
1.5
1
0.5
0
Eccentricity [-]
0
100
200
300
400
500
600
700
800
900
Elapsed Time [min]
True
TLE
Modified TLE

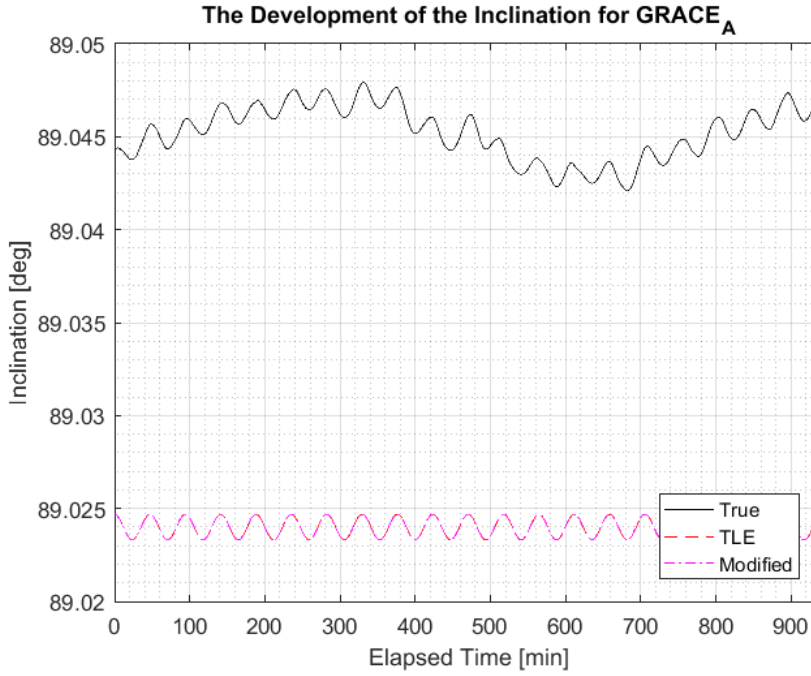
The Development of the Inclination for GRACE A
89.05
89.045
89.04
89.035
89.03
89.025
89.02
Inclination [deg]
0
100
200
300
400
500
600
700
800
900
Elapsed Time [min]
True
TLE
Modified

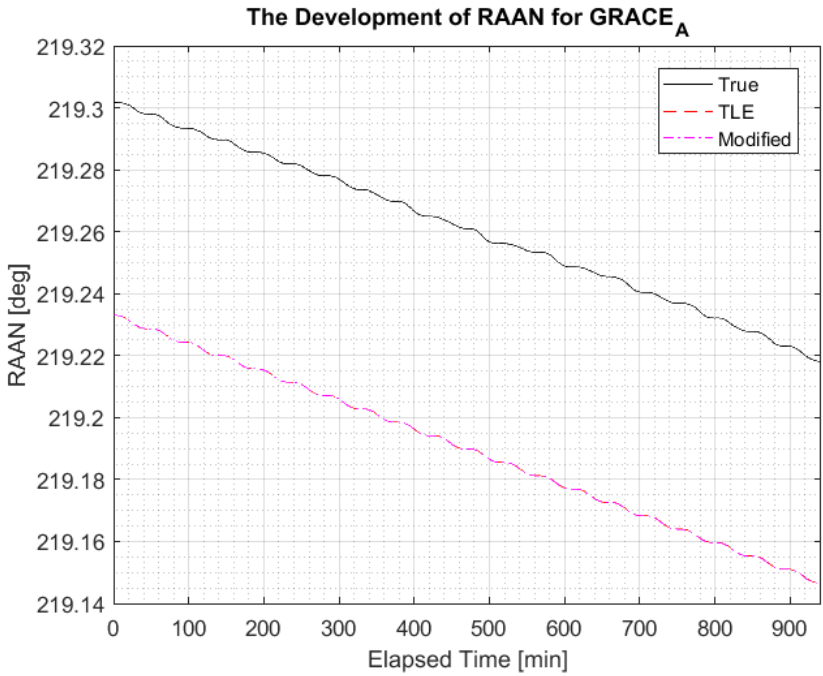
The Development of RAAN for GRACE A
RAAN [deg]
Elapsed Time [min]
True
TLE
Modified
219.32
219.3
219.28
219.26
219.24
219.22
219.2
219.18
219.16
219.14
0
100
200
300
400
500
600
700
800
900

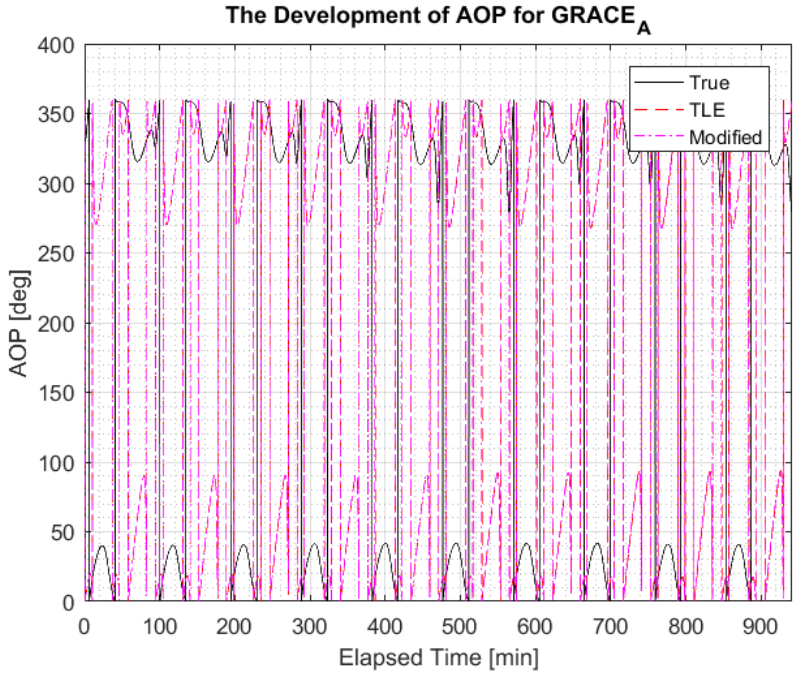
The Development of AOP for GRACE A
AOP [deg]
Elapsed Time [min]
True
TLE
Modified
400
350
300
250
200
150
100
50
0
0
100
200
300
400
500
600
700
800
900

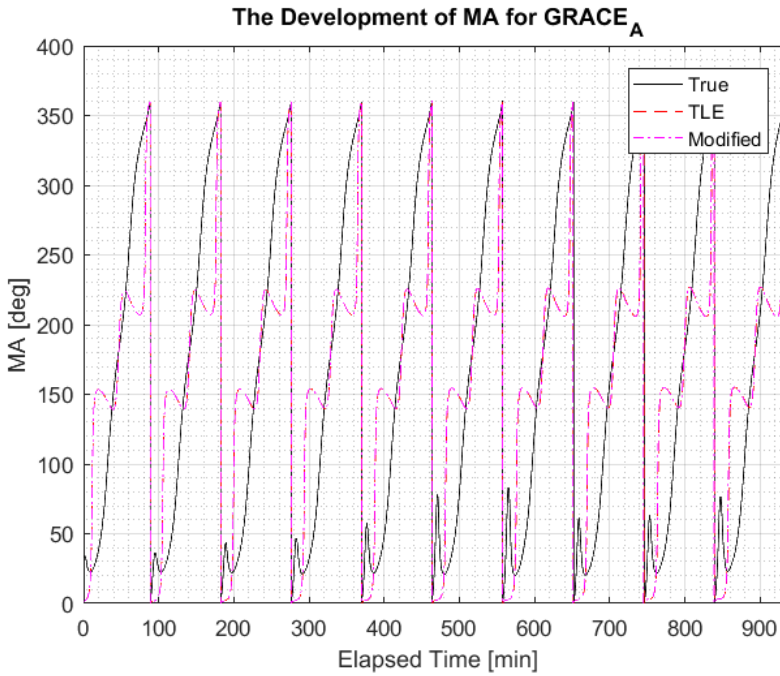
The Development of MA for GRACE A
True
TLE
Modified
MA [deg]
Elapsed Time [min]
0
50
100
150
200
250
300
350
400
0
100
200
300
400
500
600
700
800
900

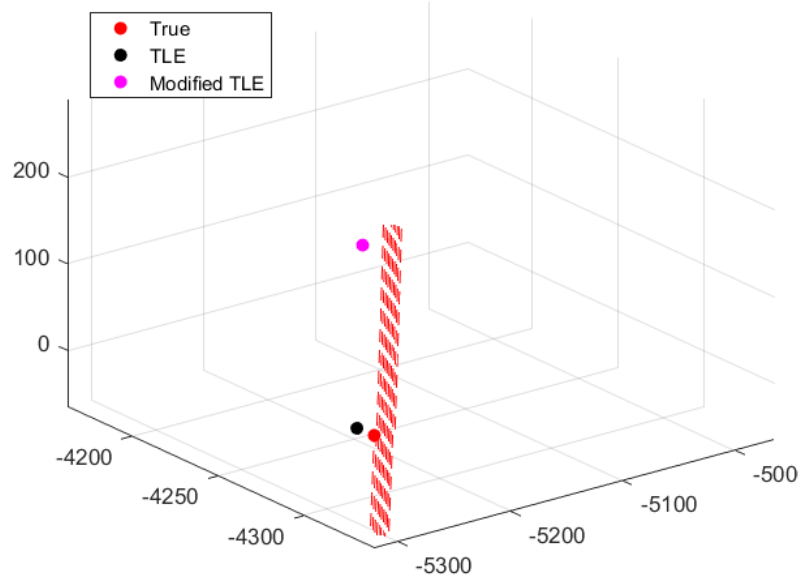
True
TLE
Modified TLE
200
100
0
-4200
-4250
-4300
-5000
-5100
-5200
-5300

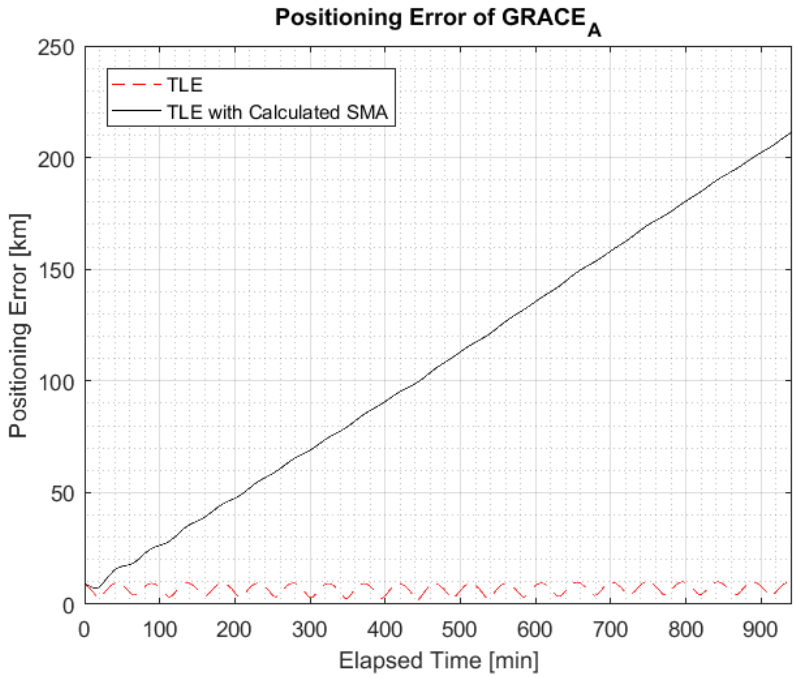
Positioning Error of GRACE A
TLE
TLE with Calculated SMA
Positioning Error [km]
Elapsed Time [min]
0
50
100
150
200
250
0
100
200
300
400
500
600
700
800
900

Appendix G. HALLEY'S METHOD

First, expand the Taylor series polynomial out to the second derivative.

$$f(x_{i+1}) = \sum_{n=0}^{\infty} \frac{f^n(x_i)}{n!}(x_{i+1} - x_i)^n$$

Now, start by looking at the individual terms. From perturbation theory, when $(x_{i+1}\text{-}x_i)$ is almost zero, the term $(x_{i+1}\text{-}x_i)^3$ becomes very small and hardly contributes to the solution. Therefore, since it almost equals zero, we can delete the third-order and higher-order terms to yield the following expression:

$$f(x_{i+1}) \approx f(x_i) + f'(x_i)(x_{i+1} - x_i) + \frac{f''(x_i)}{2}(x_{i+1} - x_i)^2$$

Using this expression, factor out an $(x_{i+1}\text{-}x_i)$, and further simplify it to

$$0 \approx f(x_i) + \left[f'(x_i) + \frac{f''(x_i)}{2}(x_{i+1} - x_i)\right](x_{i+1} - x_i).$$

From Newton's method,

$$x_{i+1} \approx x_i - \frac{f(x_i)}{f'(x_i)}$$

One of the solutions for the term $(x_{i+1}\text{-}x_i)$ is known. Therefore, take this term and substitute it into its respective place inside the brackets to obtain

$$0 \approx f(x_i) + \left[f'(x_i) + \frac{f''(x_i)f(x_i)}{2f'(x_i)}\right](x_{i+1} - x_i).$$

From here, it is only a matter of solving for x_{i+1} to arrive at Halley's Method:

$$x_{i+1} \approx x_i - \frac{2f(x_i)f'(x_i)}{2[f'(x_i)]^2 - f(x_i)f''(x_i)}$$

Bibliography

Bate, Roger R., Donald D. Mueller, and Jerry E. White. 1972. *Fundamentals of Astrodynamics.* New York, New York: Dover Publications, Inc.

Brouwer, Dirk. 1964. "Solution of the Problem of Artificial Satellite Theory Without Drag." *The Astronomical Journal* 378-396.

Curry, G. Richard. 2004. "Radar Measurement and Tracking." In *Radar System Performance Modeling*, by G. Richard Curry, 165-193. Artech House.

Doornbos, Eelco, interview by Paul Schattenberg. 2017. *Percise Orbit Determination of GOCE, GRACE-A, and CHAMP* (August).

Gill, Eberhard, Oliver Montenbruck, Kandiah Arichandran, and Timo Bretschneider. 2004. *High-Precision Onboard Orbit Determination for Small Satellites.* European Space Agency.

Goddard Space Flight Center. 2015. *General Mission Analysis Tool (GMAT).* February 27. https://opensource.gsfc.nasa.gov/projects/GMAT/index.php.

—. 2007. *General Mission Analysis Tool (GMAT) Mathematical Spefications.* Greenbelt, Maryland, United States of Americ: NASA Goddard Space Flight Center.

Hart, Roger. n.d. "Single-Station Tracking for Orbit Determination of Small Satellites." Logan, Utah, United States of America.

Hoots, Felix R., and Ronald L. Roehrich. 1980. *Spacetrack Report No. 3: Models for Propagaion of NORAD Element Sets.* Alexandria: Defense Documentation Center.

Institut National de L'information Geographique et Forestiére. 2016. *International Terrestrial Reference Frame (ITRF).* January. http://itrf.ign.fr/.

International Earth Rotation and Reference Systems Service. 2013. *Earth Orientation Data.* Accessed August 11, 2017. https://www.iers.org/.

Ismail, M. N., A. Bakry, H. H. Selim, and M. H. Shehata. 2015. "Eclipse Intervals for Satellites in Circular Orbit under the Effects of

Earth's Oblateness and Solar Radiation Pressure." *NRIAG Journal of Astronomy and Geophysics* 4 (1): 117-122.

Jäggi, Adrian. n.d. "Satellite Orbit Determination." Bern, Germany: Astronomical Institute University of Bern.

Kelso, T. S. 2014. *Orbital Propagation: Part II.* May 17. https://www.celestrak.com/columns/v01n04/.

Kozai, Yoshihide. 1959. "The Motion of a Close Earth Satellite." *The Astronomical Journal* 367-377.

Lane, M. H., and K. H. Crawford. 1969. "An Improved Analytical Drag Theory for the Artificial Satellite Problem." *American Institute of Aeronautics and Astronautics* 1-11.

Lane, Max H. 1965. "The Development of an Artificial Satellite Theory Using a Power-Law Atmospheric Density Representation." *American Institute of Aeronautics and Astronautics* 1-29.

Lane, Max H., and Felix R. Hoots. 1979. *General Pertubations Theories Derived from the 1965 Lane Drag Theory.* Alexandria, Virginia: Defense Documentation Center.

Larson, Wiley J., and James R. Wertz, . 1998. *Space Mission Analysis and Design.* 2nd. Torrance, California: Microcosm, Inc.

Lieske, Jay H. 1978. "Precession Matrix Based on IAU (1976) System of Astronomical Constants." *Astronomy and Astrophysics* 73: 282-284.

Meeus, Jean. 2009. *Astronomical Algorithms.* Richmond, Virginia: William-Bell, Inc.

Montenbruck, Oliver, and Eberhard Gill. 2000. *Satellite Orbits: Models, Methods, and Applications.* 3rd. Weßling, Germany: Springer.

NASA Orbital Debris Program Office. 2009. *Space Debris.* September 12. Accessed July 19, 2017. https://earthobservatory.nasa.gov/IOTD/view.php?id=40173.

National Aeronautics and Space Administration. 2017. *GMAT User Guide R2017a.*

National Geospatial-Intelligence Agency. n.d. *Transformatino of ECI (CIS, Epoch J2000.0) Coordinates to WGS 84 (CTS, ECEF) Coordinates.* Accessed August 8, 2017. http://earth-info.nga.mil/GandG/publications/tr8350.2/tr8350.2-a/Appendix.pdf.

National Imagery and Mapping Agency. 2000. *Department of Defense World Geodetic System 1984.* St. Louis, Missouri, United States of America: National Imagery and Mapping Agency.

Neubert, Reinhart, Ludwig Grunwaldt, and Jacob Neubert. n.d. "The Retro-Reflector for the CHAMP Satellite: Final Design and Realization." Postdam, Germany.

Park, Eun-Seo, Sang-Young Park, Kyoung-Min Roh, and Kyu-Hong Choi. 2010. "Satellite Orbit Determination using a Batch Filter Based on the Unsented Transformation." *Aerospace Science and Technology* (Elsevier) 387-396.

Psiaki, Mark L. 1999. "Autonomous Low-Earth-Orbit Determination from Magnetometer and Sun Sensor Data." *Journal of Guidance, Control, and Dynamics* 296-304.

Quality Positioning Services. 2016. *International Terrestrial Reference Frame 2014 (ITRF2014) - Knowledge Base.* July 12. Accessed August 2017. https://confluence.qps.nl/pages/viewpage.action?pageId=29856813.

Schattenberg, Paul. 2017. *An Overview on Orbit Determination Techniques for TLE Generation.* Delft, Netherlands: Paul Schattenberg.

Speretta, Stefano, Prem Sundaramoorthy, and Eberhard Gill. 2017. "Long-term performance analysis of NORAD Two-Line Elements." Delft, The Netherlands.

Staats, Elmer B. 1978. "NORAD's Information Processing Improvement Program -- Will It Enhance Mission Capability?" September 21. http://www.gao.gov/assets/130/123974.pdf.

Vallado, David A, Paul Crawford, Richard Hujsak, and T. S. Kelso. 2006. "Revisiting Spacetrack Report #3." *American Institute of Aeronautics and Astronautics.*

Vallado, David A. 2007. *Fundamentals of Astrodynamics and Applications.* Hawthorne, California: Microcosm Press.

Vallado, David A., and Vladimir Agapov. 2010. "Orbit Determination Results from Optical Measurements." Madrid, Spain.

Vetter, Jerome R. 2007. "Fifty Years of Orbit Determination: Development of Modern Astrodynamics Methods." *Johns Hopkins*

APL technical Digest. Vol. 27. no. 3. Johns Hopkins Applied Physics Labs. 239-252.

Wertz, J. R., J. T. Collins, S. Dawson, H. J. Hönigsmann, and C. W. Potterveld. 1997. "Autonomous Constellation Maintenance." Edited by Jozef C. van der Ha. *Mission Design & Implementation of Satellite Constellations.* Toulouse, France: Springer-Science+Business Media, B.V. 263-274.

Wertz, James R, Hans F. Meissinger, Lauri Kraft Newman, Geoffrey N. Smit, Robert L. Bell, John T. Collins, Simon D. Dawson, et al. 2001. *Mission Geometry; Orbit and Constellation Design and Management.* Edited by James R. Wertz, Val A. Chobotov, Michael L. DeLorenzo, Roland Doré, Robert B. Giffen, Gwynne Gurevich, Wiley J. Larson, et al. El Segundo, California: Microcosm, Inc.